ABSTRACT

Barnwell, William Garrard Distributed Actuation and Sensing on an Uninhabited Aerial Vehicle. (Under the direction of Dr. Ndaona Chokani)

An array of effectors and sensors has been designed, tested and implemented on a Blended Wing Body Uninhabited Aerial Vehicle (UAV). This UAV is modified to serve as a flying, controls research, testbed. This effector/sensor array provides for the dynamic vehicle testing of controller designs and the study of decentralized control techniques. Each wing of the UAV is equipped with 12 distributed effectors that comprise a segmented array of independently actuated, contoured control surfaces. A single pressure sensor is installed near the base of each effector to provide a measure of deflections of the effectors.

The UAV wings were tested in the North Carolina State University Subsonic Wind Tunnel and the pressure distribution that result from the deflections of the effectors are characterized. The results of the experiments are used to develop a simple, but accurate, prediction method, such that for any arrangement of the effector array the corresponding pressure distribution can be determined. Numerical analysis using the panel code CMARC verifies this prediction method.

Distributed Actuation and Sensing on an Uninhabited Aerial Vehicle

by

William Garrard Barnwell

A thesis submitted in partial fulfillment of
the requirements for the degree of
Masters of Science

Aerospace Engineering

North Carolina State University

2003

Approved by:

Dr. Ndaona Chokani
Chair of Supervisory Committee

Dr. Charles E. Hall, Jr.
Member of Supervisory Committee

Dr. Harvey J. Charlton
Member of Supervisory Committee

Biography

William Garrard Barnwell was born August 9, 1976 in Indianola, a small town in the Mississippi Delta. He has received his Bachelors and Masters of Science in Aerospace Engineering from North Carolina State University.

Acknowledgments

First, I would like to acknowledge my committee members. Dr. Chokani, my faculty advisor, is commended for his continual faith and support. Also I would like to recognize Dr. Hall who has served as co-investigator on the project and provided assistance on countless occasions. Also appreciation is given to Dr. Charlton for his devotion to mathematics and his adoration of literature.

Next, I would like to thank Stearns Heinzen for his unending support. He has been a wonderful teacher, mentor and friend.

Finally I would like to give my dedication to my fiancé and life partner Laura McCrain. Without her undying devotion and support none of this would have been possible. Thank you, Laura, may we wear white in the BR.

TABLE OF CONTENTS

LIST OF TABLES

LIST OF FIGURES

LIST OF SYMBOLS

Roman Symbols

b	Wing Span
c	Chord Length
C_l	Two-dimensional lift coefficient
C_L	Three-dimensional lift coefficient
$C_{l_{\partial a}}$	Change in lift coefficient due to aileron deflection
C_{lp}	Change in lift coefficient due to roll
C_m	Pitching moment coefficient
$C_{m_{\partial e}}$	Change in pitching moment coefficient due to elevator deflection
C_{m_α}	Change in pitching moment coefficient due to angle of attack
C_P	Pressure coefficient
L/D	Lift-to-drag ratio
p_{ss}	Steady state roll rate
Re	Reynolds Number
V_∞	Freestream velocity

Greek Symbols

α	Angle of attack
δ_a	Aileron deflection angle
δ_e	Elevator deflection angle
δ_f	Flap deflection angle
μ	Viscosity
ϱ	Density

Abbreviations

BWB	Blended Wing Body
UAV	Uninhabited Aerial Vehicle
MEMS	Microelectromechanical Systems
SMA	Shape Memory Alloy

1. INTRODUCTION

1.1 Aircraft Morphing Concepts

The National Aeronautics and Space Administration (NASA) Aircraft Morphing program has the objective of integrating research from a broad range of disciplines in order to incorporate smart technologies into high payoff aircraft applications.[1] Smart technologies may be defined as embedded actuation, sensing, and control logic that are tightly coupled in a feedback loop. Therefore, the primary focus for the Morphing program is to develop closed-loop devices having dynamic actuation, local sensing, and feedback control. Consequently, a combined approach to control systems and system identification is being used in the Morphing program to address the control laws and controller responses required for the individual devices, as well as addressing the global requirements for distributed arrays of devices that are used to achieve an overall system benefit.[2] Thus, it is within this framework that NC State and NASA have partnered to develop a flying controls test bed that is equipped with distributed actuation and sensing.

1.2 UAV Overview and Research

Uninhabited Aerial Vehicles (UAVs) are used for a wide range of purposes including military, civilian and research. In military applications, the UAV can be used for in-field reconnaissance or high altitude surveillance.[3,4] The U.S. military is also developing Uninhabited Combat Aerial Vehicles (UCAVs) to complement and/or replace fighter aircraft.[4,5] Civil use of UAVs include aerial photography and observation of traffic patterns.[6,7] In agriculture UAVs can be used to inspect crops and provide local applications of pesticide and/or herbicides.[8,9] High altitude, long range UAVs also serve as upper atmospheric weather stations.[10] Finally the use of highly instrumented UAV's in research applications provides a

quick, safe and inexpensive method to validate a wide variety of novel designs and concepts.[11,12]

New flow control methods are under investigation to reduce fuel consumption, increase range/endurance, increase control authority and enhance maneuverability throughout the entire flight envelope of an air vehicle.[13] This approach is in contrast to traditional, passive control approaches that have inherently poor performance at off-design conditions. In general, active flow control devices can yield more reduced drag, increased lift and better control of unsteady aerodynamics than passive devices.[14]

Recent activity at NC State's Flight Research Laboratory has demonstrated the advantages of highly instrumented UAVs in validating flow and flight control technologies under actual flight conditions.[15,16] In the current work an existing UAV platform is modified to evaluate multiple controller designs. An innovative replacement for traditional flaps (ailerons, elevators, rudders, etc.) is used in order to gain enhanced control of the aircraft.

1.3 Decentralized Control Techniques for Distributed Systems

New developments in decentralized control techniques have provided methods to control distributed arrays with a large number of individual elements. These techniques have been useful in a wide variety of applications. Studies have shown that the decentralized control methods provide a viable option for distributing air/ground traffic separation.[17] Several studies have investigated the robust control of multiple vehicles, including UAVs, traveling in formation and show that a decentralized control method provides optimal control while reducing the complexity of the control algorithm.[11,18] Furthermore, recent discoveries in material science and fluidics have been used to create a variety of shape-change and fluidic effector devices to enable new approaches to aerospace vehicle flight

control. Microelectromechanical systems (MEMS) make feasible the concept of combining actuation, sensing, computing, and telecommunications to produce a very large array of distributed configurations with unprecedented capabilities for control.[19] Future aerospace vehicles might use distributed arrays with hundreds of such devices for stabilization and maneuver control, thereby augmenting or replacing conventional ailerons, flaps and/or rudders.[20]

The underlying theme in each of the distributed systems is that standard control techniques have severe limitations because the overall system is rich and complex, and requires high levels of connectivity and massive computations.[21] However, many systems contain similar elements that interact with their nearest neighbor in a simple and predictable fashion. The goal of developing decentralized control techniques is to obtain tractable algorithms for controlling the simple systems and then applying the technique to a more vast, overall scheme.

The current work develops a test-bed with a distributed actuation and sensing suite that provides the capability to test and evaluate a large number of controllers and control methods, such as decentralized control. Control objectives include active separation control, stabilization and maneuver control, disturbance rejection or upset recovery, mission-adaptive performance enhancement, and failure accommodation.[13] In addition to the aforementioned control objectives, reduced fuel consumption, enhanced maneuverability and reconfigurablity are potential benefits of distributed effector and sensor arrays.[24,25] Sophisticated controller designs using elegant inputs, such as modal shapes that only vary amplitude and frequency across the effector array will be used to provide multi-axis aircraft control.

1.4 NASA Morphing Wing

The Smart Wing program was developed and sponsored by DARPA, AFRL and NASA. The program evaluated smart materials through a multi-disciplinary investigation for high payoff aircraft.[22] Phase 1 of the Smart Wing program concluded with wind tunnel testing in 1997. One aspect of the Smart Wing design was a Shape Memory Alloy (SMA) actuated trailing edge device that replaced a traditional control surface. This design produced a contoured wing, or a hingeless control surface (Figure 1).[23] The benefits of a contoured wing are illustrated in Figure 2. The conventional hinged flap, due to its abrupt change in curvature, is more prone to separation than the smooth transition of the contoured control surface. Figure 2 shows that the contoured wing yields a higher value of the maximum lift coefficient, $C_{l,max}$, thus increasing the stall envelope of the aircraft. Another benefit is an increase in the upper corner of the drag bucket, which indicates an increase in L/D_{max}.

Wind tunnel testing of the Smart Wing was conducted at NASA Langley's 16 ft Transonic Dynamic Tunnel on a 16% scale F/A – 18 E/F model. The model was tested with both the traditional, hinged control surfaces and the contoured, SMA actuated surface. The Smart Wing showed significant aerodynamic improvements.[24] Figure 3 shows that for any given angle of attack, α, there is an increase in the lift coefficient, C_L, resulting in 8% increase in lift. The pressure distribution around the airfoil, Figure 4, shows that the Smart Wing produces increased amount of suction on the upper surface near the trailing edge of the airfoil. This increase in negative pressure directly contributes to the increased lift. The Smart Wing also shows improved aerodynamic performance by using the contoured wing design.

1.5 Objectives of Project

The current project develops a UAV test-bed to test decentralized control methods using a distributed array of contoured control surfaces. The effector and sensor suite are designed to evaluate, in the future, a wide range of control objectives. The implementation of the distributed effector array is illustrated in Figure 5. The continuous control surface proved very difficult to manufacture; therefore, in the current work the effector array is approximated with a series of segmented and independently actuated effectors. Surface pressure measurements will be used as sensors for the array. A recent study has shown that as few as four pressure measurements on an airfoil can provide information on the overall lift.[25] Thus the pressure sensors are designed to provide feedback in the controllers. Each effector is paired with a single sensor; therefore, the effector/sensor pair forms a subsystem. Each subsystem is first characterized and then the subsystems are used to predict the response for the more complete effector/sensor array.

2. EXPERIMENTAL AND NUMERICAL APPROACH

2.1 Experimental Set-Up

2.1.1 *Wind Tunnel*

The NC State Subsonic Wind Tunnel is a closed return wind tunnel with a test section 32" high * 45" wide * 46" long. The wind tunnel operates at a maximum dynamic pressure of 12 lb/ft^2; thus the maximum velocity is approximately 85 ft/s. The tunnel is equipped with Plexiglass® side walls at the test section. A solid door was constructed to replace one of the Plexiglass® side walls. This door is equipped with a 6" offset splitter plate onto which the model is mounted. The splitter plate is used to eliminate the influence of the wind tunnel walls' boundary layer on the model and to position the model in the center portion of the test section.

2.1.2 *Instrumentation*

2.1.2.1 *Pressure Measurement System*

Two pressure scanning devices are used to measure the surface static pressures on the model. A Scanivalve© system equipped with 96 channels and a ±3.5" H_2O transducer is used as the primary pressure measurement system. A Pressure Systems, Inc. Electronic Scanning Pressure (ESP) module was also used. The ESP module has 16 independent ±10" H_2O transducers that are contained within a lightweight and compact case; this module is capable of measuring up to 32 channels.

2.1.2.2 *Servo Serial Boards*

Servo serial boards, manufactured by BASIC-X™ are used to command the positions of the servos/effectors. The boards allow the command of 256

positions for each servo. Up to eight serial servo boards can be linked together therefore providing independent control of up to 64 servos using a single serial connection.

2.1.3 UAV *BWB Delta*

The testbed is the UAV *BWB (Blended Wing Body) DELTA* that was designed, built and flight tested at NC State (Figure 6). The flying wing platform is similar to the design of the NASA BWB.[26] The root chord and tip chord are 58" and 5 ¼", respectively. The 9.5' wingspan aircraft is powered by an Aviation Microjet Technology™ (AMT) mini-turbojet engine that is rated at 18-lbf static thrust.[27,28] The cruise and stall speeds are 120 ft/s and 45 ft/s, respectively. The UAV has no landing gear; instead the aircraft is dolly-launched and skid recovered. The aircraft has a dry weight of 30 lb. with a payload capacity of 15 lbs. *BWB DELTA* is an ideal candidate for the effector array because the flying wing design allows the trailing edge surfaces of the aircraft to provide pitch and/or roll control. The UAV *BWB DELTA* has removable outboard wing panels; therefore, new wing panels equipped with the distributed effectors were constructed.

2.1.4 *Wing Panels*

The outboard wing panels of the aircraft have a 21" root chord with a 5 ¼" tip. The airfoil section is a NACA 0015. The wing span is 31 ¼". Figure 7 shows details of the wing during construction. The skins for the wings are made of a wet-laminate fiberglass/graphite composite which incorporates a 1/8" Korex™ honeycomb core. The internal formers are 1/8" birch plywood. Aluminum bars are integrated into the skin to provide attachment points for the effectors. A hatch provides access to all of the servo motors, effectors, and pressure ports.

Twelve effectors, adjacent to each other, are installed on each wing. The effector #1 is at the root and effector #12 is 18" from the root. Because of the thin cross-section at the most outboard portion of the wing, a conventional hinged control surface is installed. A second conventional control surface is located on the main body section of the aircraft. Thus the arrays of distributed effectors are backed-up by conventional surfaces which give redundancy to the control surfaces of the aircraft. Figure 8 shows the starboard wing with the complete distributed effector array.

Each outboard wing panel equipped with the distributed effectors, servos and other hardware has a weight of 3.5 lbs. The baseline wing panels have a weight of 2.25 lbs. Thus, the net increase in the weight of the wings is 1.5 lbs. There are additional power requirements to operate the 24 servos (one for each effector); however, the additional batteries are used to replace the ballast that is required in the nose of the aircraft. Thus the overall weight increase of the modified wing panels and its accessories is less than the available payload weight of 5 lbs.

2.1.5 ***Distributed Effectors and Sensors***

2.1.5.1 *Effectors*

The arrays of independently actuated surfaces, also termed effectors, are designed to operate with the same bandwidth (1-2 Hz) and maximum deflection (±15º) as the conventional control surfaces. Therefore the modified vehicle can operate similar to the baseline vehicle when the effectors are deployed as a conventional surface.

The actuation of the effectors is provided by commercially available, off-the-shelf servo motors, Hobbico™ CS-5 nano-servos. The design of the effectors incorporates a hingeless, contoured control surface. Each effector is comprised of two rectangular elements of thin spring steel having dimensions of 0.007"

(thickness), 1.5" (width) and 4" (length), one each on the upper and lower surfaces. The effectors are deflected by the servos through a pull-pull wire linkage; the opposing surface restores the actuated surface to its neutral position. An undeflected and deflected full-scale prototype of an effector is shown in Figure 9.

2.1.5.2 *Sensors*

An array of 24 surface pressure taps (12 taps per wing) is used to monitor the deflections of the effectors. One pressure tap, 0.040" in diameter, is located 4.05" from the trailing edge of each effector. The pressure taps are equally spaced at intervals of 1.5" in the spanwise direction with the first pressure tap located 0.75" from the root chord. Therefore there is one pressure tap located immediately forward of each effector. The pressure tubulations are connected to the pressure scanning system through 0.040" diameter nylon tubing.

2.2 Computational Methods

2.2.1 *XFOIL*

The effect of Reynolds number, flap hinge location, and flap deflection are examined using XFOIL. XFOIL is a two-dimensional inviscid analysis code based on the linear vorticity stream function.[29] In the present work an airfoil, whose undeflected cross-section is the NACA 0015, is examined. The CAD program, Unigraphics™, is used to generate undeflected and deflected trailing edge airfoil sections. The contour of the modified wing panel is modeled by the deflected trailing edges of the airfoil section. A range of deflected airfoil sections with hinge locations of x/c = 0.4-0.9 and flap deflection angles of 10-60° are examined.

2.2.2 *CMARC*

The aerodynamic analysis code CMARC is used to examine the pressure distribution on the UAV *BWB DELTA* equipped with the array of distributed effectors. CMARC is a three-dimensional, inviscid, panel code method based potential flow theory.[30] The geometry of the UAV, with and without deflection of the effectors, is modeled in Unigraphics™. A representative aerodynamic model of the wing panels is shown in Figure 10; the inset shows a close-up of the deflected effectors.

3. RESULTS AND DISCUSSION

Numerical and experimental results of the performance of the distributed effector and sensor are presented in this chapter. The performance is first examined using the two-dimensional analysis code XFOIL (3.1); then a three-dimensional analysis using CMARC (3.2) is presented; finally the results of an experimental wind tunnel investigation are presented (3.3).

3.1 XFOIL Results

The outboard wing panel of UAV *BWB DELTA* is tapered. This variation in the geometry results in different cross-sections across the span of the effector array. XFOIL provides a quick method to isolate the effect of the varying geometry by examining two-dimensional, airfoil, cross-sections of the wing. This analysis delineated the influence of changing flap deflection, Reynolds Number and hinge location. Also the potential aerodynamic benefits of a contoured design versus a conventional hinged flap are examined.

3.1.1 Effect of Flap Deflection

Figure 11 shows the effect of changing flap deflection, δ_f. Three airfoils with deflections of 10°, 15° and 20° deflections are presented. The hinge location is $x/c = 0.7$ and the Reynolds number is $1x10^6$. The lift and pitching moment coefficients are plotted versus angle of attack, α. As the deflection angle is increased, the C_l is larger for a given angle of attack, while $C_{l,max}$ is unchanged. Thus, the flow over the effectors is neither separated nor stalled even at large deflection angles. This is verified by the fact that the pitching moment coefficient remains constant for all cases.

3.1.2 Effect of Reynolds Number

Figure 12 shows the results for the change in Reynolds number for an airfoil with a deflection of 15° and hinge location x/c = 0.7. Reynolds Number is defined as:

$$\mathrm{Re} = \frac{\rho V c}{\mu} \tag{3.1}$$

Thus the chord length, c, is proportional to the Reynolds Number. The chord length of the airfoil cross-section varies from 19" (inboard) to 8" (outboard) due to taper in the wing. The Reynolds Number varies from 1 $x10^6$ - $2.5x10^6$ across the span of the effector array at the cruise velocity of the aircraft (120 ft/s). The results show that although the Reynolds number changes considerably there is little effect on the aerodynamic performance of the airfoil. The section lift coefficient, C_l, differs only slightly near stall and the pitching moment coefficient, C_m, shows very little deviations for all cases.

3.1.3 Effect of Hinge Location

Figure 13 shows XFOIL results for airfoils with various hinge locations. Each effector has a different hinge location, because the chord of the wing changes, but the length of each effector is 4". Thus the hinge location varies from $x/c \approx 0.8$ for the inboard effector to $x/c \approx 0.5$ for the outboard. Each of the airfoils has a 15° deflection with a Reynolds Number of $1x10^6$. Since the chord length is proportional to increasing the Reynolds Number, Figure 12, shows varying the chord length will not change the results.

The results show that the outboard effectors in the array provide a greater C_l for a given angle of attack, α. However, this also suggests the onset of stall, defined as $C_{l,max}$, will occur at a lower α for the outboard effectors. Therefore, although the outboard effectors are the most effective, they stall first, and the aircraft is more susceptible to wing tip stall. This tip stall of the aircraft has been has been

previously observed in the wind tunnel analysis of a sub-scale model and in the initial vehicle flight testing; the present XFOIL analysis clarifies these previous results.[28] The only slight variations in pitching moment due to the hinge location occur at negative angles of attack that are unobtainable by the aircraft; it is thought that this variation does not change with hinge location.

3.1.4 Effect of Surface Geometry

The NACA 0015 airfoil with a conventional, hinged control surface and the contoured airfoil are next examined. Figure 14 shows the comparison for a 15º flap deflection at a Reynolds Number of $1x10^6$ and a hinge location of $x/c = 0.7$. C_l and C_m of the contoured airfoil are increased compared to the conventional airfoil at any given angle of attack; therefore, there is a clear benefit in the performance of the airfoil that utilizes the contoured trailing edge. Similar results are also obtained by varying flap deflection, Reynolds Number and hinge location for the two airfoils. These results agree very well with the wind tunnel observations in the Smart Wing program (Figure 3). The wind tunnel results for the Smart Wing show an increase in lift coefficient of approximately 8%; whereas, the XFOIL analysis shows improvements of approximately 10%. The improvement in pitching moment also suggests that there are considerable improvements in the control authority of the contoured control surface.

Although the magnitude increase in C_l compare well, the pressure distributions from the XFOIL analysis differs from the wind tunnel results for the Smart Wing. The Smart Wing shows an overall increase in suction mainly due to an increase at the trailing edge location (Figure 4). However, the results from XFOIL show that the suction spike produced by the sharp transition at the flap deflection is flattened out, while there is an overall increase in the magnitude of the upper surface pressures (Figure 15 and Figure 16). This overall increase in magnitude is what accounts for the lift improvement for the contoured airfoil.

The improvement in lift is significant, and possibly could be even greater if the gap between the traditional surface and airfoil is also modeled. The gap may cause greater flow separation, and degrade the performance; whereas, the modified airfoil very closely represents the manufactured design.

In summary, the analysis shows that the effectors can be used in a wide range of conditions without degradation to the performance. The study further suggests that the array of effectors will have additional aerodynamic benefits due to the contoured geometry of the design.

3.2 CMARC Results

3.2.1 Control Power Analysis

The CMARC simulations are used to provide an inviscid, three-dimensional analysis of the UAV. The CMARC analysis reported in Ref(27) provides the baseline information for control power effectiveness of the control surfaces. The trailing edge surfaces of the UAV are designed to provide pitch and roll control; therefore, the two figures of merit used to evaluate the control power effectiveness for roll and pitch are p_{ss} and $d\alpha/d\delta_e$, respectively. The following equations are used to calculate the control power estimates:

$$\text{Elevator Control Power} = \frac{d\alpha}{d\delta_e} = \frac{C_{m_{\partial e}}}{C_{m_\alpha}} \tag{3.2}$$

$$\text{Steady State Roll} = p_{ss} = -\frac{2C_{l_{\partial a}} V_\infty}{C_{lp} b}\Delta\delta_a \tag{3.3}$$

Previous UAV research at NC State has shown good aircraft handling qualities are obtained for values of p_{ss} near 360°/s and $d\alpha/d\delta_e$ between 1 - 2.[31]

The control power of the effector array, predicted by CMARC analysis, ascertained that the modified control surfaces can provide adequate control of the aircraft.[32] The analysis determined the amount of control power the effector array could provide without the assistance of the conventional surfaces. The pitch and roll authority the baseline vehicle, modified vehicle, and the effector array are shown in Figure 17 andFigure 18. The results show the vehicle outfitted with the effector array provides similar control authority to the baseline vehicle. Therefore, the modified vehicle with the effectors deployed as conventional surfaces result in handling that is similar to the baseline vehicle. A modal deflection, where the spatial distribution of tip deflections form a sine wave whose peak amplitude is 15°, is also examined. The control power is comparable to that of the baseline vehicle. Figure 17 andFigure 18 also show the control power estimates using only the effector array; it is seen that the effector array provides up to half the control power.

The effector array provides a good measure of pitch and roll authority without use of the conventional surfaces. During a flight test scenario all surfaces are used in a conventional manner for the more difficult maneuvers such as takeoff, approach and landing. Once a holding flight pattern is established at altitude, the conventional surfaces are disabled and the ability of the effector array to navigate the aircraft and perform simple maneuvers can be examined. Following the flight test the conventional surfaces can be re-engaged and the vehicle landed with a conventional control surface configuration.

3.2.2 Pressure Characterization

Figure 10 shows the CMARC panel model; in the inset of a close-up of a deflected effector is shown. The symmetry along the centerline of the aircraft simulates the presence of the sidewall in the wind tunnel tests. The CMARC model of the wing determined the pressure response to a single effectors

movement. Finally, a sensitivity matrix related the pressure response for multiple effectors movements.

3.2.2.1 Single Effector Movement

CMARC yields predictions of the aerodynamic coefficients, such as lift coefficient by calculating the pressure at each panel and then integrating to find the aerodynamic coefficients. Therefore, the pressure at the panel nearest to the location of the pressure sensor can be compared to the measurement of the pressure sensor.

Figure 19, shows a plot of the CMARC pressure distribution; the inset shows effector #3 at a 10° deflection. CMARC analysis with no effector deflections provides the baseline data. The baseline data set is subtracted from the predicted pressure with the deflected effectors. The baseline data is used as a reference to determine the net change in pressure due to the displacement of the effectors. The following equation is used to quantify the pressure change, ΔC_P,

$$\Delta C_P = C_{P,\mathrm{Re}corded} - C_{P,Baseline} \tag{3.4}$$

The change in pressure on all sensors is measured for +5° and +10° deflections of each effector. Since the wing has a symmetric airfoil section, the pressures on the upper and lower surface for both positive and negative deflections are obtained in a single run. Figure 20,Figure 21 and Figure 22 show the pressure response for deflections of an inboard (#3), a mid-span (#6), and an outboard effector (#10). In general, the change in pressure varies linearly with deflection.

Thus, the pressure response to a single effector at any deflection angle can be predicted. It is observed that the sensor nearest to the actuated effector is most sensitive to the deflection. This sensitivity decreases for sensors further away

from the actuated effector; the sensitivity is negligible more than three sensors away from the actuated effector.

3.2.2.2 Multiple Effector Movement

The change in pressure due to the actuation of a single effector, $\frac{d(\Delta C_P)}{d\delta_f}$, is the slope of the linear fit shown in Figure 20-Figure 22. These slopes, sensitivity coefficients, are plotted in Figure 23 for three representative cases. They can also be summarized in a matrix of the form:

$$A = \begin{matrix} a_{11} & a_{12} & \cdots & a_{1N} \\ a_{21} & a_{22} & \cdots & a_{2N} \\ \vdots & \vdots & \ddots & \vdots \\ a_{N1} & a_{N2} & \cdots & a_{NN} \end{matrix} \tag{3.5}$$

where $a \equiv \frac{d(\Delta C_P)}{d\delta_f}$, and the row and column numbers represent the effector and sensor numbers, respectively. The sensitivity coefficients derived in this manner from the CMARC analysis are shown in Table 1. The results in Table 1 and Figure 23 confirm that the most sensitive sensor is that which is nearest to the actuated effector. Also, the neighboring sensors equidistant to the actuated effector have approximately the same response to deflection of the effector.

The results above also suggest that the distributed actuation and sensing array could be used for failure monitoring and fault detection. Specifically, each effector configuration is uniquely related to the pressure distribution of the sensors. Therefore, for a given effector configuration, an inconsistency in the pressure distribution can be used to identify a faulty sensor. Conversely for a

measured pressure distribution, an inconsistent effector indicates the possible failure of an effector.

3.3 Wind Tunnel Results

Figure 24, shows a representative series of effector configurations in the wind tunnel that were evaluated during the testing. Three modal shapes with varying spatial frequency and a one-up-one-down configuration are shown. The purpose of the wind tunnel tests is to access the ability to characterize the pressure response due to the actuation of a single effector and then for actuation of multiple effectors.

3.3.1 *Single Effector Characterization*

Initially the wind tunnel experiments followed the same test matrix as the CMARC analysis. A single effector was deflected over a range of angles and the pressure response was measured. Figure 25,Figure 26 andFigure 27 show the results for a representative inboard (#3), mid-span (#6) and outboard (#10) effector moved through a ±15° degree sweep. The effectors are displaced with two degree increments to provide good resolution for the linear curve fit. The results are similar to the CMARC simulations. The change in pressure with respect to deflection of an effector is linear. The magnitudes of the pressure changes are also comparable to the CMARC analysis. As was previously observed the largest sensitivity is measured at the sensor closest to the actuated effector. The neighboring pairs of equidistant also show a similar response. The slopes of the linear fit to the data are summarized in the sensitivity matrices shown in Table 2.

The sensitivity coefficients from the CMARC analysis and the wind tunnel results are shown for three representative cases in Figure 28, Figure 29 andFigure 30. The results from the wind tunnel show that the CMARC simulations over predict

the pressures for the sensor that is closest to the actuated effector, but at the neighboring sensors the experiment and CMARC are in good agreement. The source of error could be attributed to the wake separation between the main wing and the actuated effector in the CMARC modeling. Nonetheless, the results provided a method to estimate the pressure change due to the actuation of a single effector using experimental or numerical data.

3.3.2 *Multiple Effector Characterization*

The effect of flap deflection on the change in pressure can be written in matrix form as:

$$Ax = b \tag{3.5}$$

The sensitivity coefficients a_{nn} in matrix A are given in Table 1 andTable 2 for the CMARC analysis and the wind tunnel experiment, respectively. The vectors x and b are given as

$$x = \begin{matrix} \delta_{f1} \\ \delta_{f2} \\ \vdots \\ \delta_{f(N-1)} \\ \delta_{fN} \end{matrix} \tag{3.6}$$

and

$$b = \begin{matrix} \Delta C_{P1} \\ \Delta C_{P2} \\ \vdots \\ \Delta C_{P(N-1)} \\ \Delta C_{PN} \end{matrix} \tag{3.7}$$

where x is a vector of flap deflections and b is a vector of change in pressure coefficient. The matrix equation therefore provides a method to combine the effects of the actuation of a single effector into the actuation of multiple effectors.

Figure 31Figure 38 show the predicted and measured pressure response for several commanded effector deflections. The prediction method is evaluated in each wing for several effector deflections including modal shapes with varying frequency, constant deflection angles, and one-up-one-down configurations. The prediction method uses Equation 3.5 to estimate the pressure response. The results show that the linear combination of the single effectors provides a reliable prediction for the multiple effector deflections for a range of effector deflections.

The above results show that the distributed effector/sensor array has the capability to meet many of the proposed mission objectives. All of the elements for closed loop control within the bandwidth limitations of the sensors and actuators are in place. Specifically, for a given effector position there is a measurable response from sensors. Therefore effectors can be commanded to a desired configuration whose resultant pressure distribution optimizes a particular flight condition, such as maximum L/D. The feedback can be potentially used for stabilization and maneuver control, disturbance rejection or upset recovery. The overall performance of the vehicle can be improved because the effector array can be actively controlled to optimize several phases of the flight regime, such as take-off, landing and cruise.

3.3.3 UAV Readiness for Flight Testing

The distributed effector and sensor array has been designed, manufactured, tested and installed. Figure 39 shows UAV *BWB DELTA* equipped with the distributed effector and sensor array. The UAV is therefore ready to enter the

flight testing phase of the project. Final evaluations of the system which included effector calibrations and comparison of the in-flight and wind tunnel pressure monitoring systems have also been conducted.

3.3.3.1 Effector Calibrations

A servo is employed to actuate each effector. The deflection angle, for a given servo position may differ; due to slight manufacturing inconsistencies, physical taper in the wing and the varying tension in the wire linkages. Therefore, a calibration of servo position versus deflection angle was made for each effector. Figure 40 shows a graph of the calibrations for the port wing. Effectors 1-6 have a slope of equal magnitude, but opposite sign, of effectors 7-12; this is because the separate banks of servos are mounted in opposite directions (Figure 7). Table 3 summarizes the calibration results for both wings. These calibrations are incorporated into a look-up table that may be used in a flight computer system to command an effector to a specific deflection angle.

3.3.3.2 Comparison of Pressure Systems

Figure 41 shows a comparison of the measured pressures using the two pressure monitoring systems used during the wind tunnel testing. The Scanivalve™ system is a mechanically multiplexed, pressure system permanently mounted the wind tunnel; the ESP module is a compact lightweight, electronically multiplexed system that will ultimately be used for in-flight pressure measurement. The results show that both systems provide identical results. Thus, the ESP module is suitable to be used as the pressure monitoring system during the flight testing portion of the project.

4. CONCLUDING REMARKS

4.1 Summary of Results

This study examines the effectiveness of multi-axis control of a UAV using a distributed actuation and sensing array that was designed, manufactured and analyzed. XFOIL and CMARC are used to computationally evaluate the design, and then wind tunnel tests are used to experimentally validate the design.

XFOIL provides a two-dimensional numerical analysis of the effects of flap deflection, Reynolds Number, and hinge location. This analysis is used to demonstrate the performance benefits of a contoured surface in the design of the effectors. The distributed array consists of 24 effectors that is 12 on each wing. The resulting effector is comprised of two plates of spring steel having dimensions 4" (chord) x 1.5" (span) x 0.007" (thickness). The effectors are actuated by a hobby servo via antagonizing pull-pull linkages. The pressure sensors, centered at the base of each effector, are located on the upper surface of the wing. An array of 24 pressure sensors provides feedback information for the system.

Subsequent three-dimensional analysis using CMARC provides comparisons of the control authority for the baseline vehicle equipped with conventional surfaces to the control authority of the modified vehicle equipped with the effector array. The modified vehicle has comparable control authority in addition to the advantages of distributed effectors. These advantages include fault tolerance, failure monitoring, and aeroelastic tailoring.

Wind tunnel testing provides an experimental evaluation of the performance of the effector array. The measured effects of the deflections compare well with the

CMARC simulations. The simulated and measured pressures, in response to the deflections of a single effector, are used to develop a simple but accurate method to determine the pressure distribution that results from deflections of multiple effectors.

4.2 Continuing Research

At the time of writing this thesis, wind tunnel testing of the fully equipped UAV is underway at the NASA-Langley 12' Wind Tunnel. The purpose of the test is to access the static and dynamic performance of the actuation and sensing suite. Preliminary results are encouraging and indicate that flight testing would be beneficial.

4.3 Recommendations for Future Work

Following the wind tunnel testing at NASA the UAV will be readied for flight testing. The present study and the wind tunnel tests at NASA provide a experimental and numerical database that can be used as the basis for multiple controller designs. The envisaged flight test plan includes the demonstration of closed loop, multi-axis control using the distributed effector and sensor arrays.

5. TABLES

Table 1: Sensitivity Matrix from CMARC

Sensor # / Effector #	1	2	3	4	5	6	7	8	9	10	11	12
1	64.80	38.72	20.48	12.64	8.88	6.88	4.16	4.12	3.48	2.92	2.50	2.96
2	41.00	49.15	37.86	18.44	11.30	8.14	4.74	4.62	3.86	3.16	2.72	3.18
3	21.32	33.37	94.88	39.48	17.74	10.94	5.80	5.38	4.30	3.48	2.92	3.40
4	13.18	16.80	38.02	85.96	35.78	17.92	7.86	6.64	5.06	3.90	3.14	3.64
5	9.26	10.11	17.34	34.10	54.02	37.70	13.10	9.02	6.36	4.72	3.62	4.12
6	7.08	7.12	10.54	17.46	35.74	62.08	27.70	14.08	8.74	6.04	4.48	4.92
7	5.58	5.22	6.66	8.66	12.46	23.64	78.32	45.68	20.60	11.82	7.84	7.90
8	4.60	4.25	5.20	6.34	8.06	11.64	27.72	95.80	48.52	20.76	11.74	10.52
9	4.14	3.72	4.44	5.18	6.14	7.66	9.22	30.36	94.94	48.50	20.96	15.66
10	3.86	3.43	4.06	4.52	5.18	6.06	5.80	11.54	30.24	95.88	48.86	26.70
11	4.00	3.54	4.12	4.52	4.94	5.60	5.10	8.02	12.32	30.80	98.22	57.92
12	4.10	3.65	4.14	4.48	4.82	5.38	4.80	6.96	8.82	13.14	31.72	113.2

** Note: All Values *1x10^5

Table 2: Sensitivity Matrix for
Starboard and Port Wing Matrices of
$\frac{d\Delta C_P}{d\delta_f}$

Starboard

Effector # \ Sensor #	1	2	3	4	5	6	7	8	9	10	11	12
1	49.22	26.94	13.12	8.48	6.31	4.71	1.64	-0.02	2.84	0.87	1.64	0.04
2	27.66	55.24	32.90	17.18	10.98	7.05	3.31	2.01	4.01	1.71	2.65	1.08
3	17.49	31.27	60.35	38.43	19.25	11.50	5.83	3.82	4.57	3.44	3.22	1.68
4	12.01	17.97	35.10	68.70	37.86	19.71	9.51	5.62	6.36	4.34	3.44	2.50
5	8.13	10.15	17.18	33.11	46.12	32.19	10.97	8.07	7.02	4.56	3.84	2.23
6	3.82	5.76	10.87	20.03	32.95	52.94	14.53	8.57	4.10	-1.20	-1.77	-5.93
7	6.42	1.04	5.19	11.72	15.85	32.19	28.88	27.33	19.04	13.04	10.37	8.05
8	5.68	3.47	5.39	9.27	11.45	17.86	25.77	38.09	30.84	19.73	13.34	9.78
9	5.04	4.98	5.54	8.17	11.51	14.30	16.25	33.04	56.73	41.21	25.44	16.01
10	4.39	4.96	5.51	6.96	10.11	12.06	12.00	22.79	40.21	56.26	44.13	26.59
11	4.71	4.84	4.86	6.54	9.17	10.38	9.72	14.57	23.45	31.88	50.42	39.61
12	3.88	4.43	4.68	5.68	7.86	8.31	8.14	11.14	18.49	22.59	36.12	59.42

Port

Effector # \ Sensor #	1	2	3	4	5	6	7	8	9	10	11	12
1	55.21	34.25	21.63	15.04	6.08	-4.53	3.66	4.08	3.64	2.49	-1.68	2.75
2	36.31	59.25	39.92	23.85	13.32	1.28	6.77	7.17	4.39	4.56	0.65	5.05
3	23.15	38.07	63.78	40.97	22.90	9.27	10.24	11.76	6.78	6.89	-1.53	4.83
4	17.13	22.30	37.05	57.57	37.02	14.23	10.97	10.87	4.39	3.31	-3.49	2.03
5	11.22	15.73	24.36	38.55	66.44	34.73	14.54	9.00	3.09	-0.15	-0.06	-1.53
6	11.22	11.59	17.08	23.87	39.58	57.17	22.94	17.86	10.15	7.52	6.44	4.68
7	5.20	7.37	11.03	13.38	16.37	26.37	46.44	38.96	22.02	15.85	9.80	9.33
8	5.21	7.43	8.18	10.81	13.77	18.08	29.31	55.01	34.77	22.88	11.26	10.97
9	4.63	6.21	8.76	9.43	11.16	12.23	18.54	36.38	48.79	36.64	25.30	15.17
10	4.77	5.67	7.45	8.34	8.50	8.94	12.82	24.23	31.14	54.29	37.73	25.60
11	5.51	6.83	7.73	8.36	8.69	7.28	10.55	19.51	23.81	32.57	40.19	36.71
12	3.57	6.24	6.50	7.44	8.23	6.71	9.89	17.39	17.66	22.99	29.06	55.28

** Note: All Values *1x10^5

Table 3: Calibrations for Effector
Deflections from -15 to 15 degrees

Port Wing

	-15	-13	-11	-9	-7	-5	-3	-1	0	1	3	5	7	9	11	13	15
1	45	60	71	81	90	98	108	116	119	121	127	131	139	145	153	161	170
2	49	65	75	83	92	100	108	116	118	121	127	132	139	147	154	163	173
3	30	62	67	74	81	91	100	109	113	117	127	131	138	145	151	161	170
4	43	62	71	81	89	100	108	118	121	127	137	141	147	157	161	167	177
5	55	64	74	86	94	104	111	120	123	126	134	141	146	156	162	164	174
6	57	69	79	89	97	108	116	122	124	131	141	145	150	162	168	171	177
7	206	195	179	169	158	150	143	136	133	128	119	115	105	99	92	85	75
8	201	193	183	173	161	153	145	136	130	127	120	110	103	97	86	77	69
9	206	194	183	174	163	153	145	138	133	129	120	111	104	97	88	80	69
10	204	189	178	170	158	151	142	133	129	125	118	110	104	94	84	76	66
11	200	172	163	153	143	135	127	121	119	115	117	99	95	87	81	72	61
12	206	186	175	163	154	144	135	128	125	122	112	107	102	94	86	76	66

Starboard Wing

	-15	-13	-11	-9	-7	-5	-3	-1	0	1	3	5	7	9	11	13	15
1	184	181	173	168	158	151	143	136	132	129	122	115	106	98	88	77	63
2	188	180	170	162	152	144	138	131	126	124	117	111	102	94	86	75	64
3	189	179	167	159	149	142	134	128	124	122	116	109	102	94	87	78	65
4	193	181	171	162	151	145	137	131	126	124	119	110	102	93	84	74	61
5	193	182	171	164	152	147	138	132	127	125	119	111	104	96	88	77	66
6	189	178	168	160	149	144	136	128	125	121	114	105	97	88	80	69	61
7	66	81	95	102	115	118	126	133	135	139	143	154	161	170	177	188	204
8	70	87	99	105	115	118	124	131	132	138	142	152	160	164	173	181	190
9	63	85	97	104	113	117	121	130	132	136	141	150	158	161	170	177	187
10	60	84	94	102	110	115	118	127	129	134	138	148	155	158	167	171	179
11	57	79	92	104	111	117	121	130	132	137	142	151	159	162	172	178	187
12	54	75	86	99	108	118	123	133	137	142	149	160	168	171	178	184	188

6. FIGURES

Figure 1: SMA Actuated Smart Wing
Contoured Surface

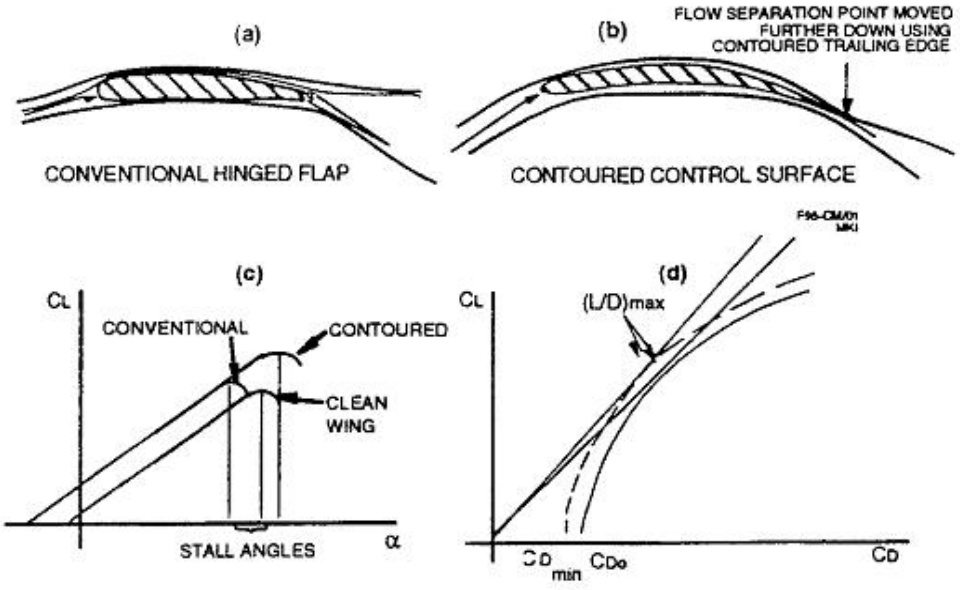

Figure 2: Comparison of Contoured
and Conventional Control Surfaces

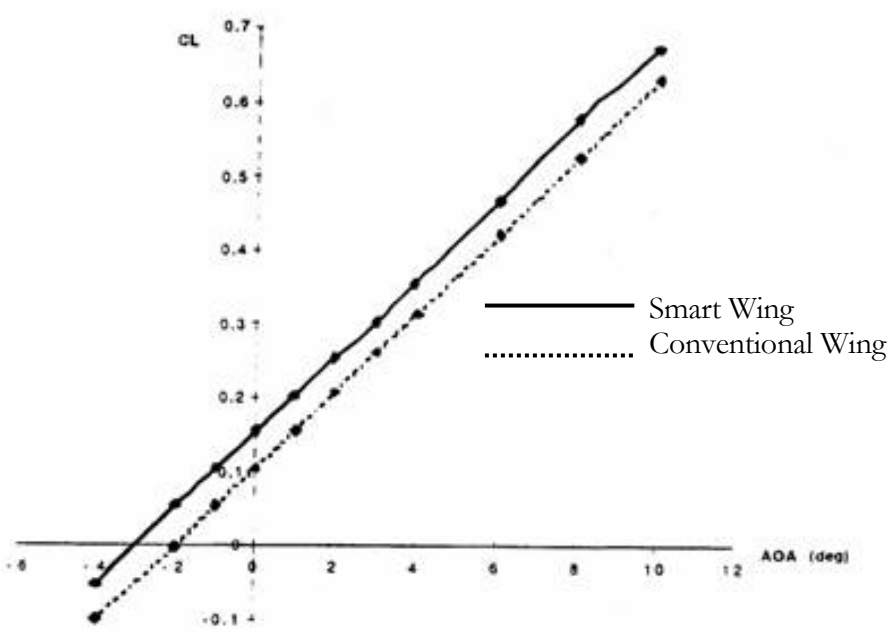

Figure 3: CL vs. AOA Runs for Smart Wing and Conventional Surface

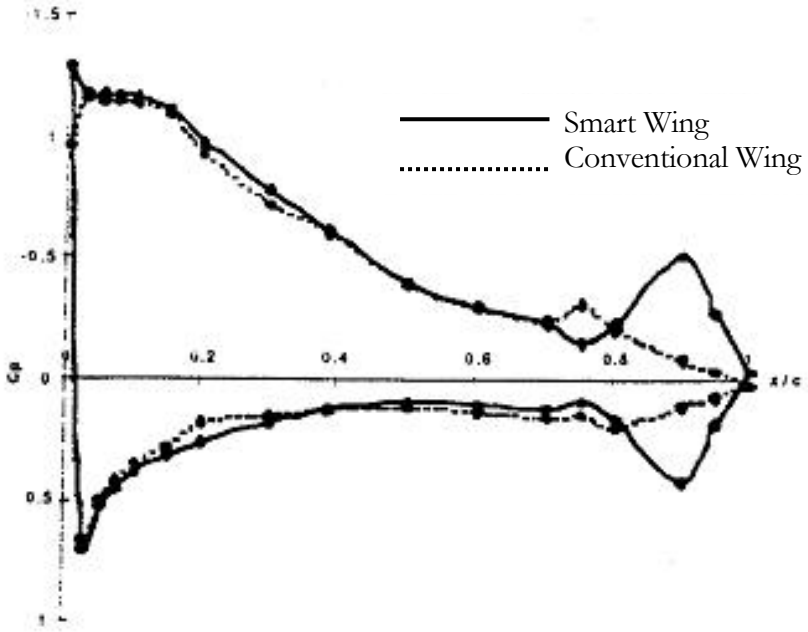

Figure 4: Cp Pressure Distribution for
Smart Wing and Conventional Surface

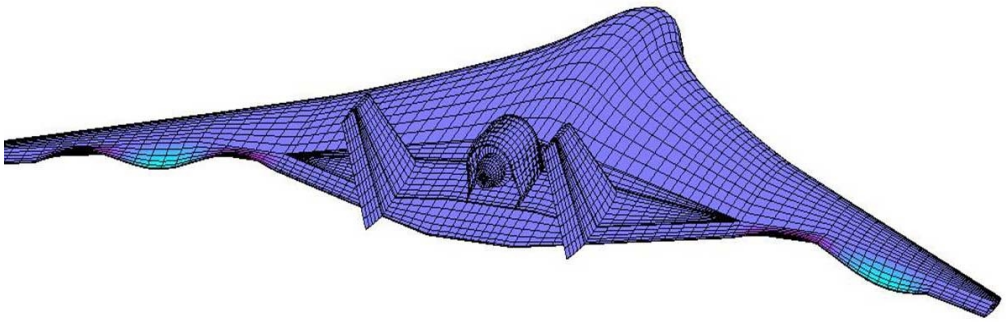

Figure 5: Theoretical Effector Array

Figure 6: UAV BWB DELTA

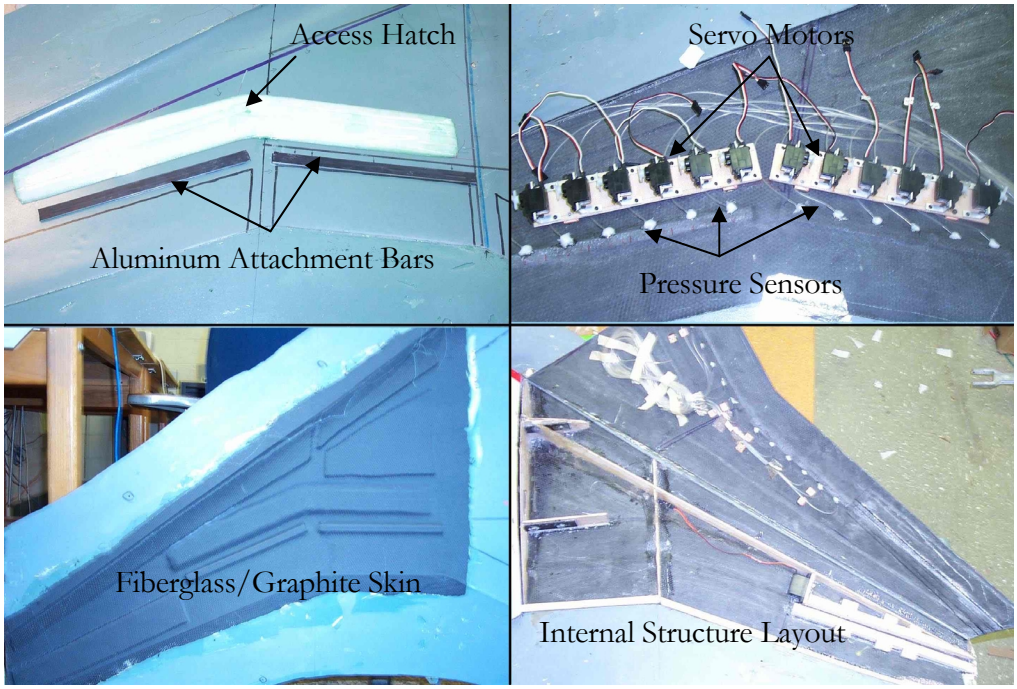

Figure 7: Construction History of
Outboard Wing Panels

Figure 8: Starboard Wing with
Effectors Attached

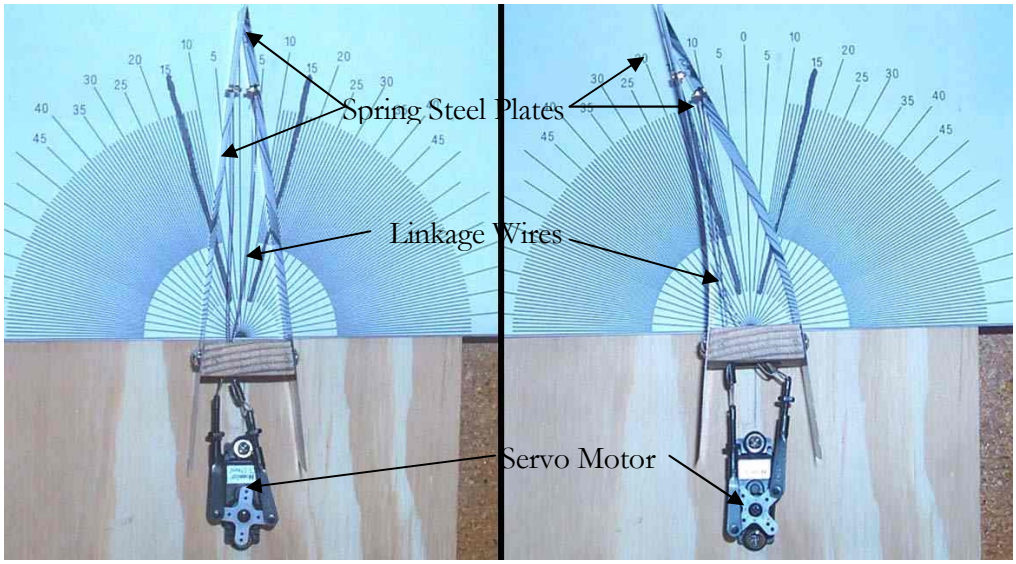

Figure 9: Actuator Design - Deflected (left) and Undeflected (right)

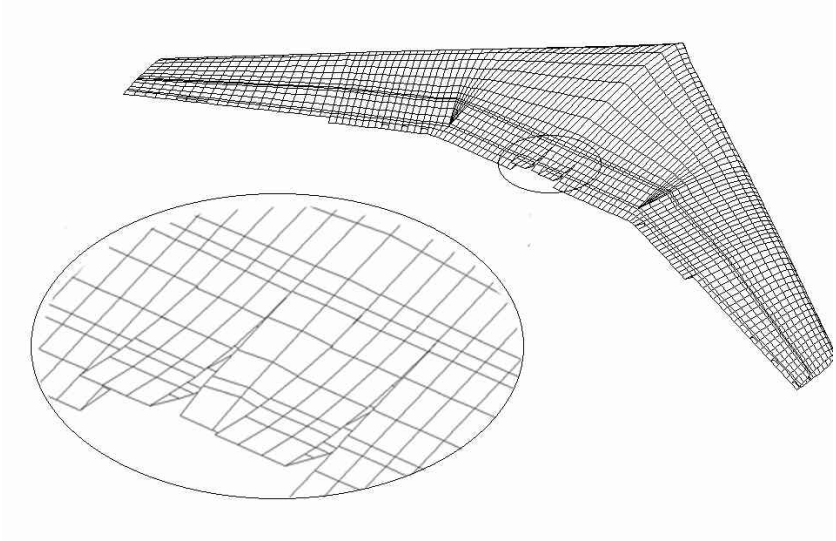

Figure 10: CMARC Model of Outboard Wing Panel with Effector Deflection

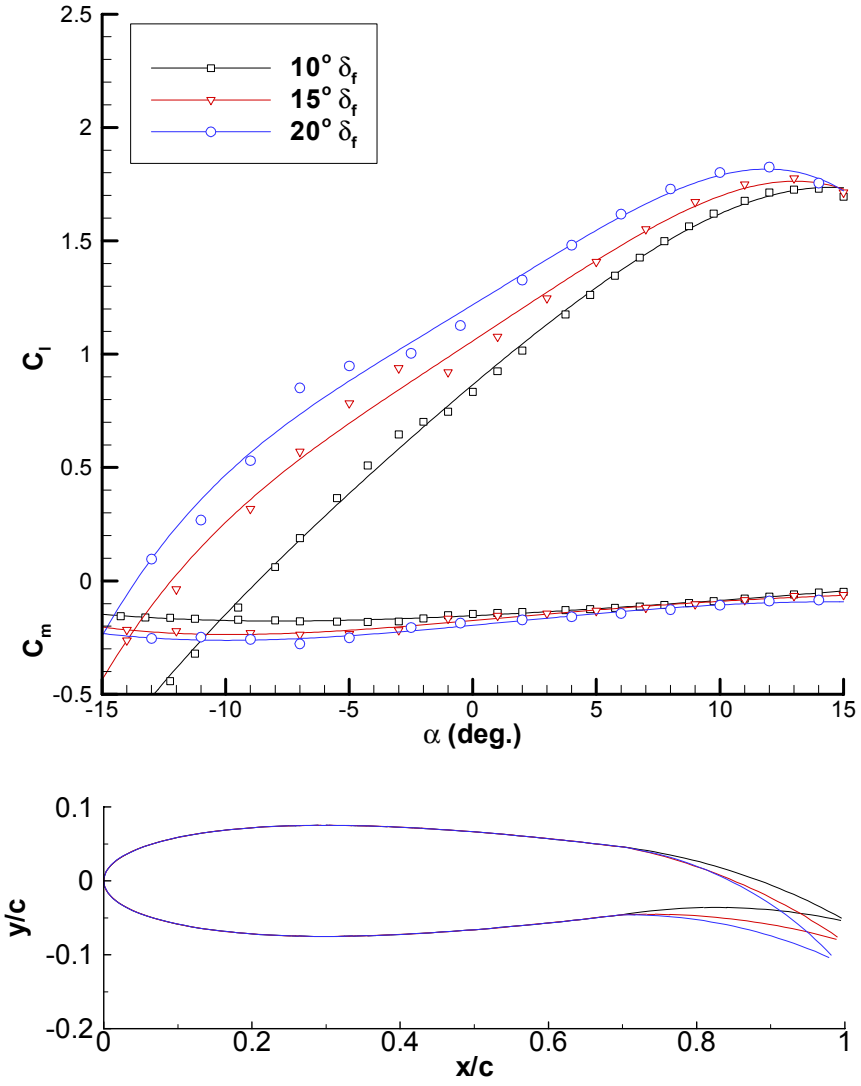

Figure 11: Effect of Flap Deflection
on Aerodynamic Performance

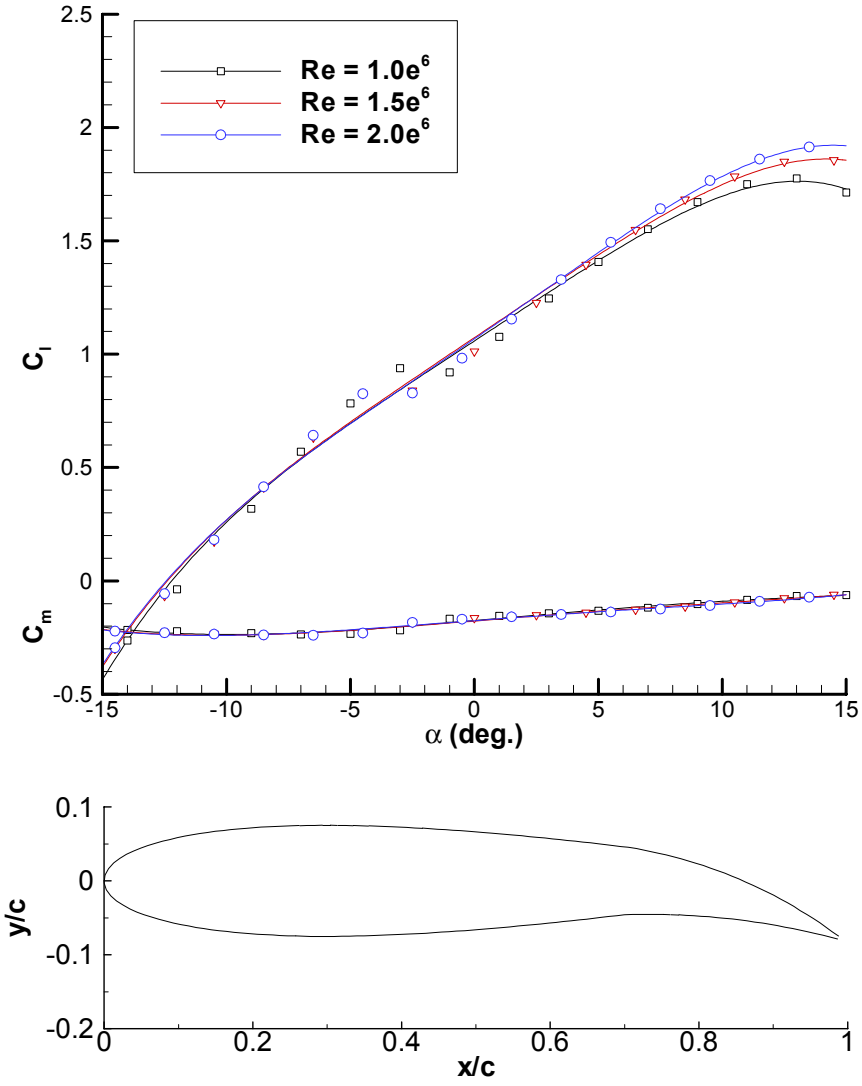

Figure 12: Effect of Reynolds Numbers on Aerodynamic Performance

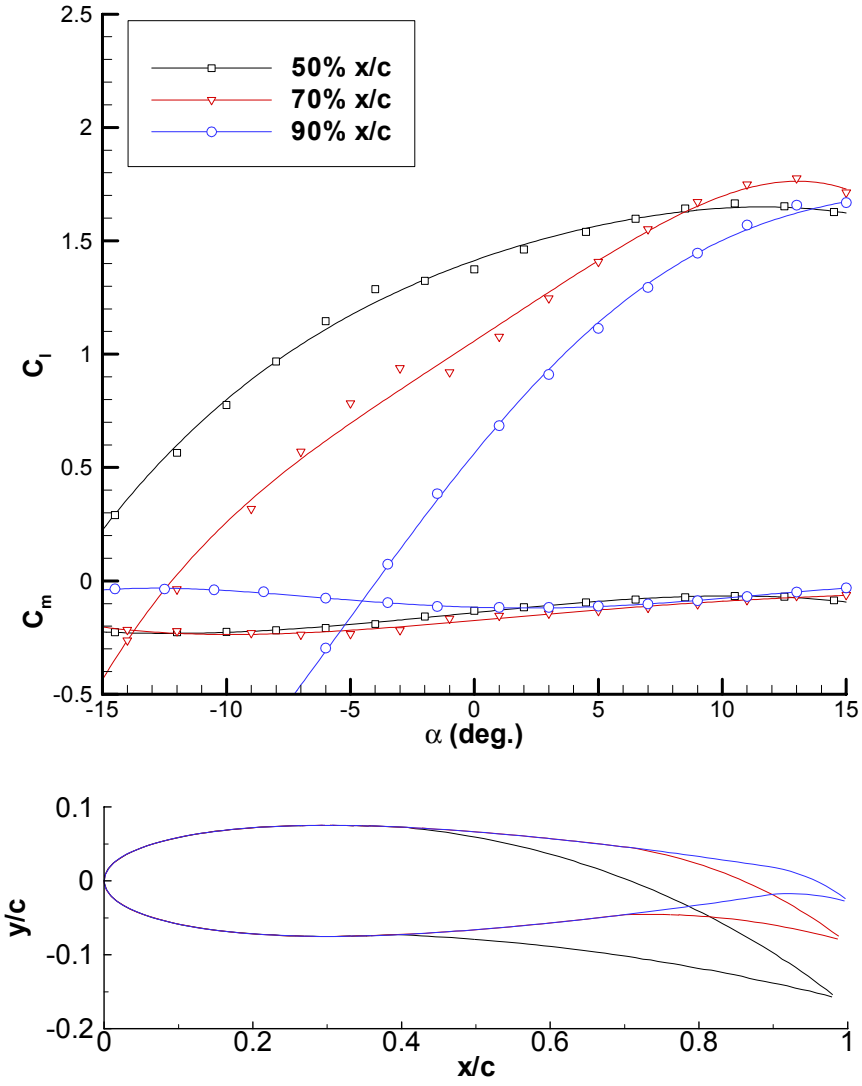

Figure 13: Effect of Hinge Location
on Aerodynamic Performance

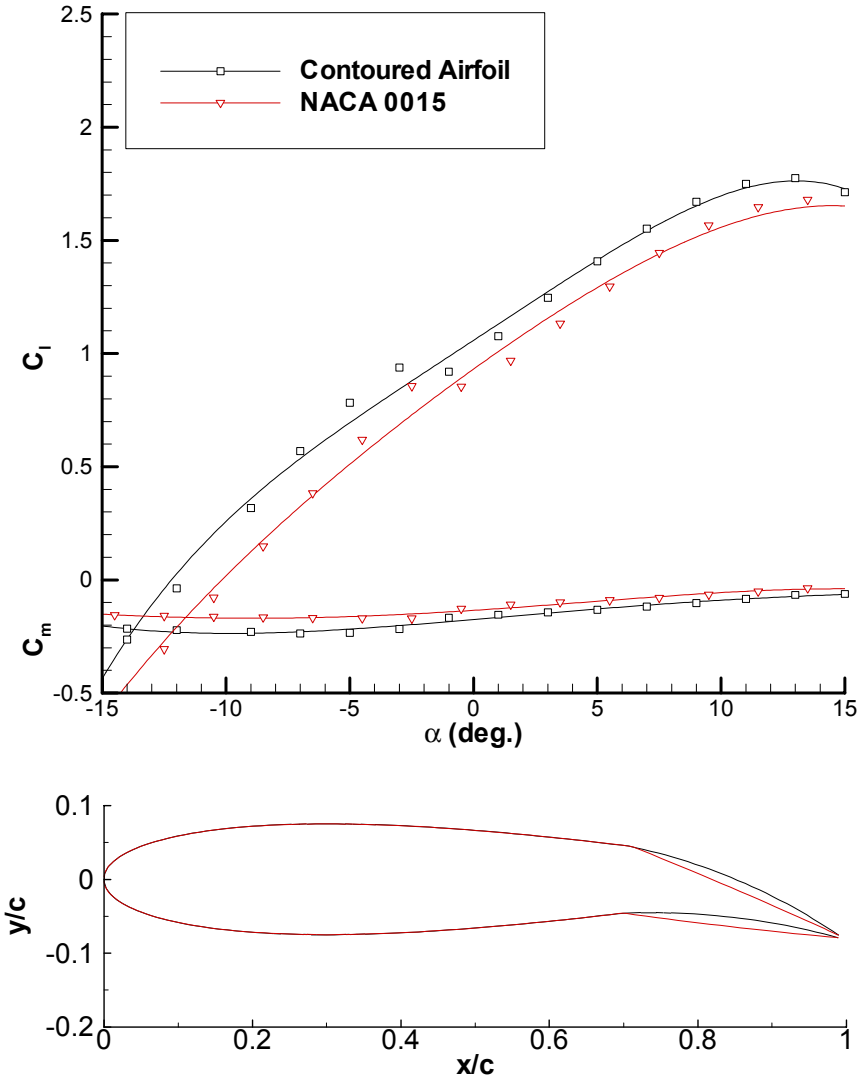

Figure 14: XFOIL Analysis of
Conventional and Contoured Surfaces

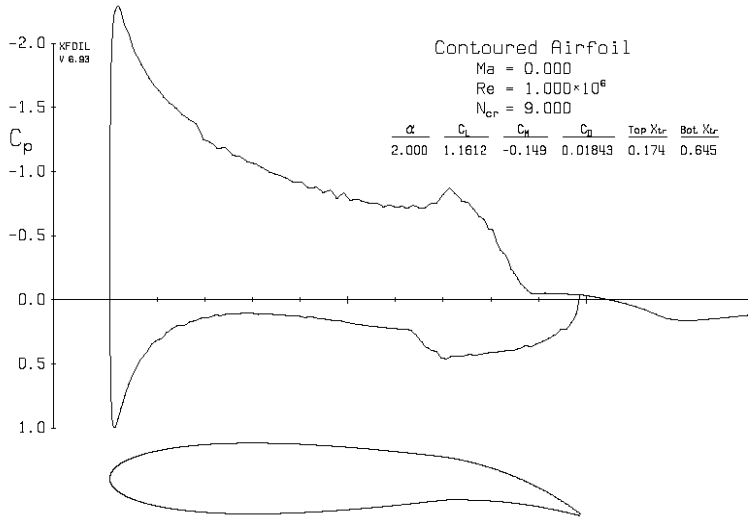

Figure 15: XFOIL Plot of Coefficient of Pressure vs. x/c for Contoured Airfoil

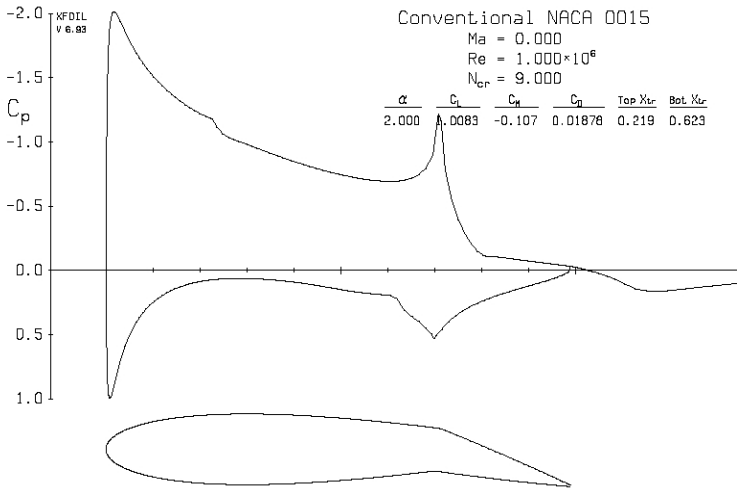

Figure 16: XFOIL Plot of Coefficient of Pressure vs. x/c for Conventional Airfoil

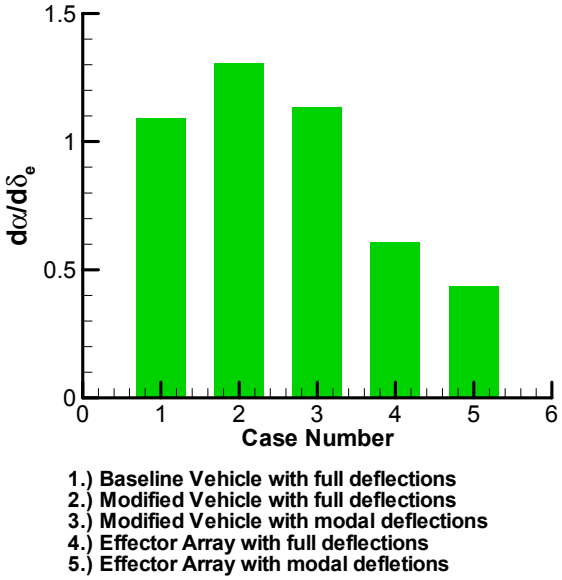

Figure 17: Elevator Control Powers

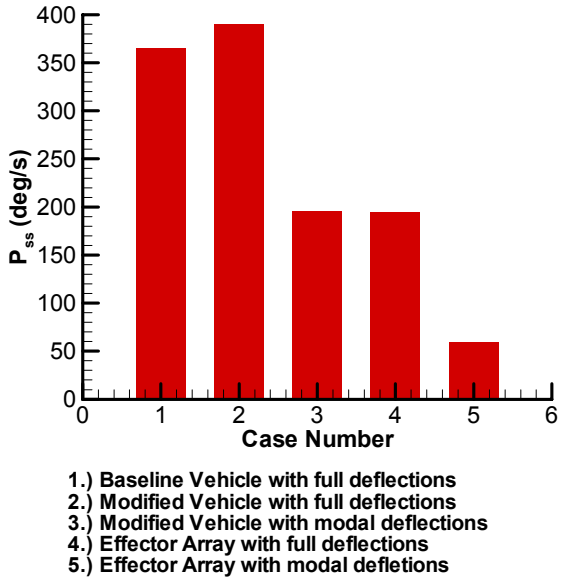

Figure 18: Steady State Roll Rates

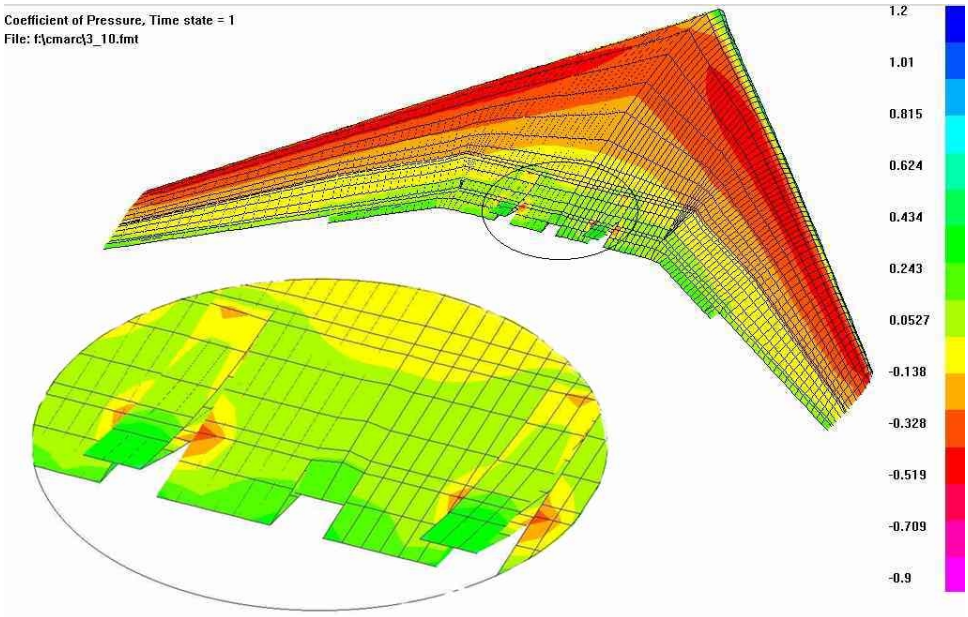

Figure 19: Pressure Distribution from CMARC with an inset of a deflected effector

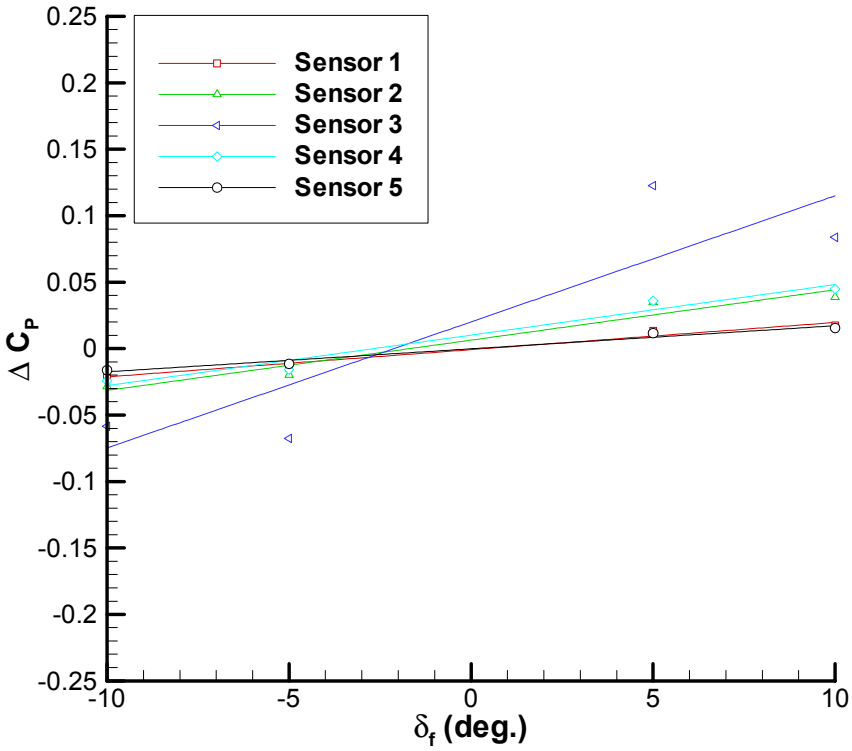

Figure 20: CMARC Pressure Response for Inboard Effector Movement (#3)

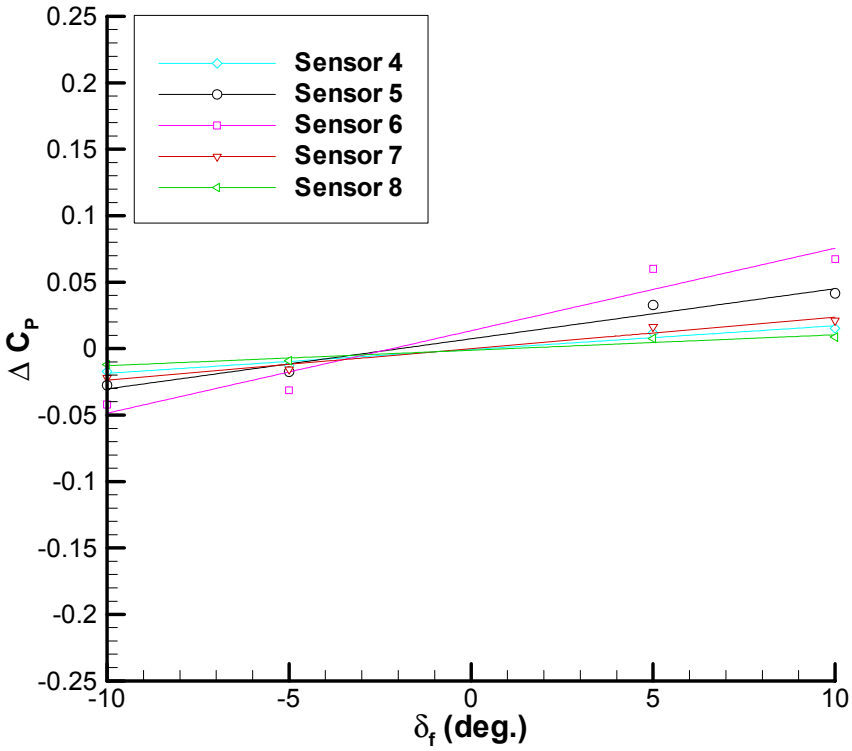

Figure 21: CMARC Pressure Response for Inboard Effector Movement (#6)

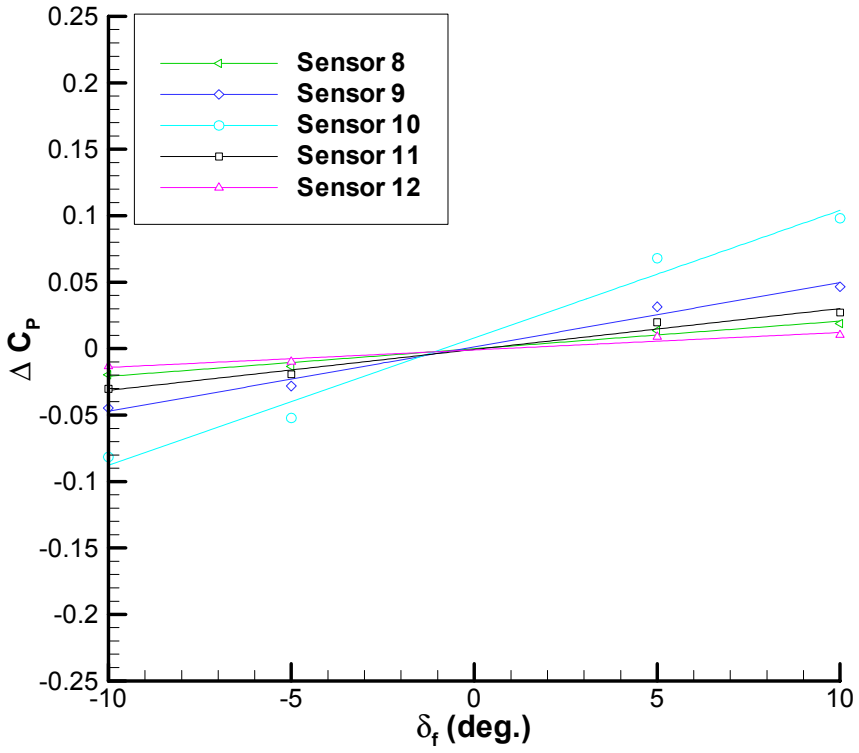

Figure 22: CMARC Pressure Response for Inboard Effector Movement (#10)

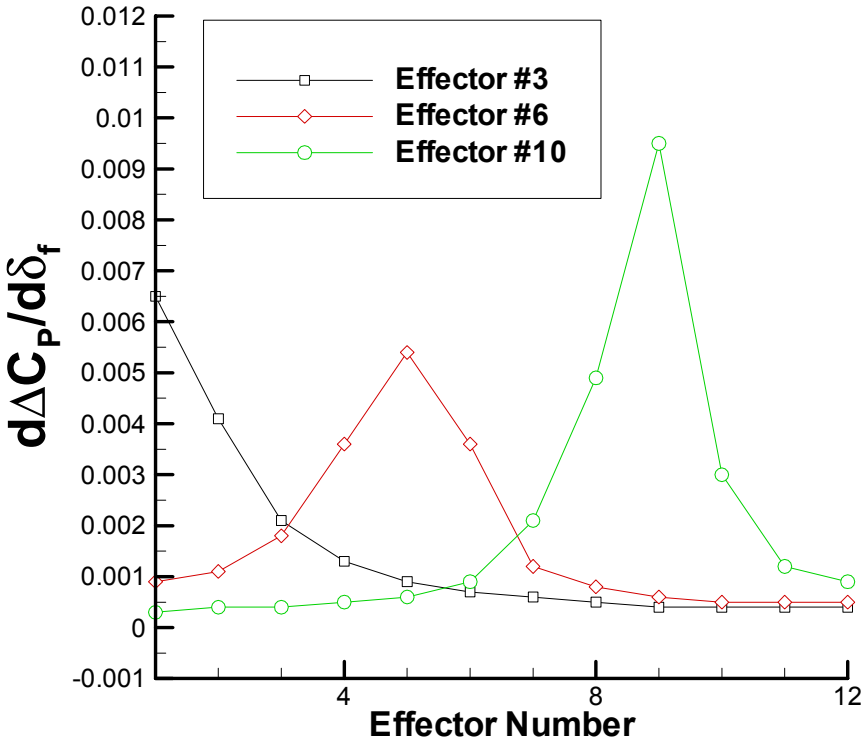

Figure 23: CMARC Sensitivity Coefficients

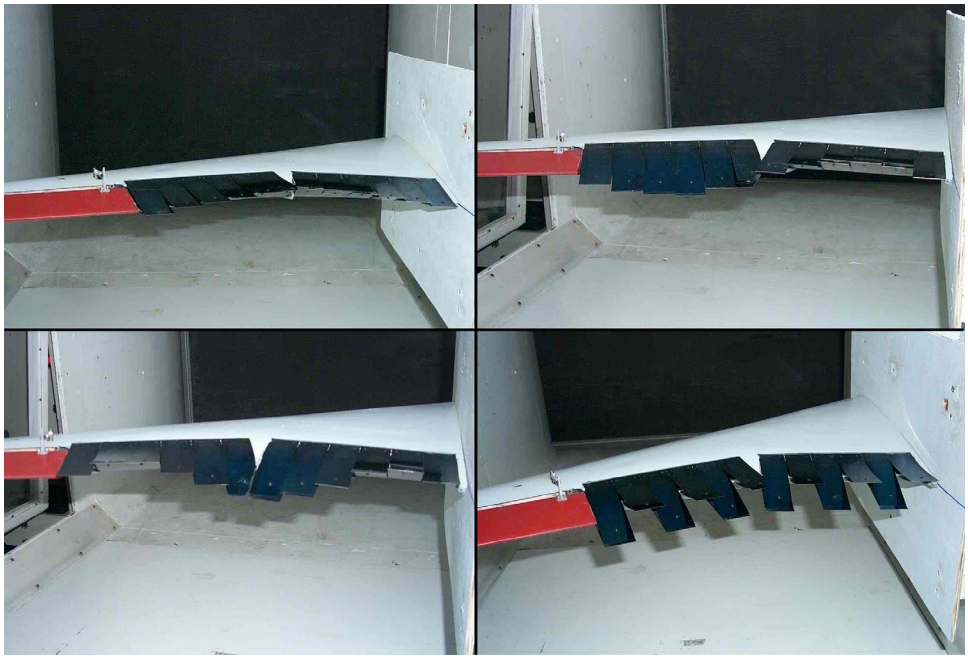

Figure 24: Port Wing in Wind Tunnel
with Various Effector Arrangements

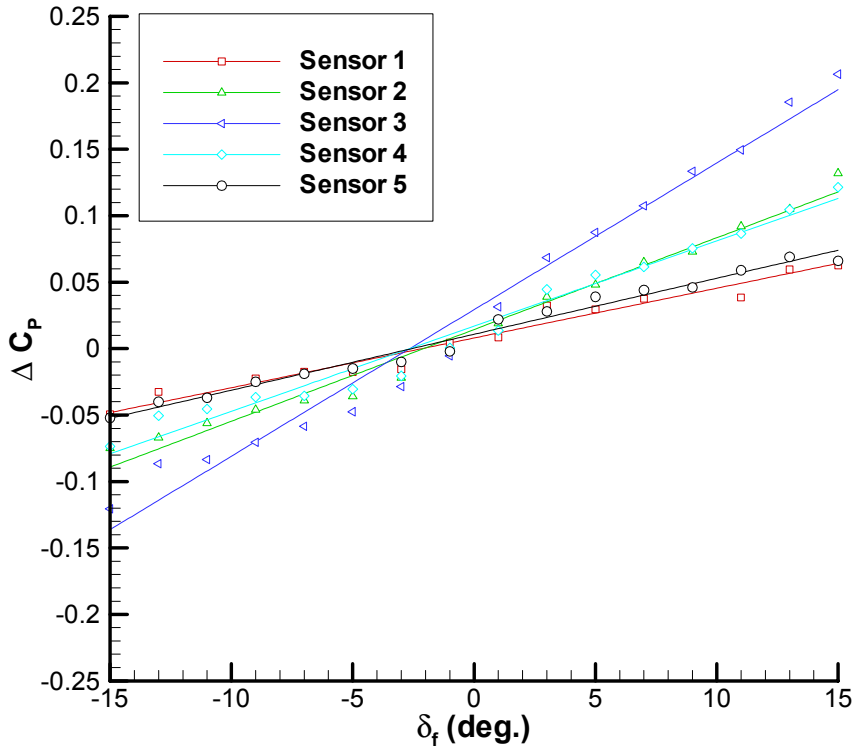

Figure 25: Pressure Response for
Inboard Effector Movement (#3)

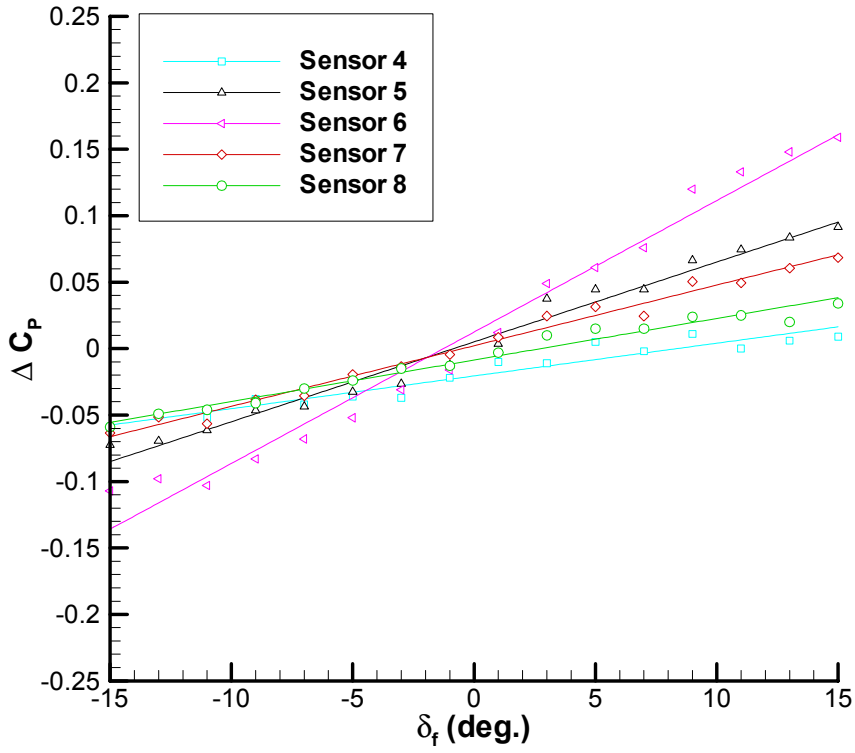

Figure 26: Pressure Response for Mid-Span Effector Movement (#6)

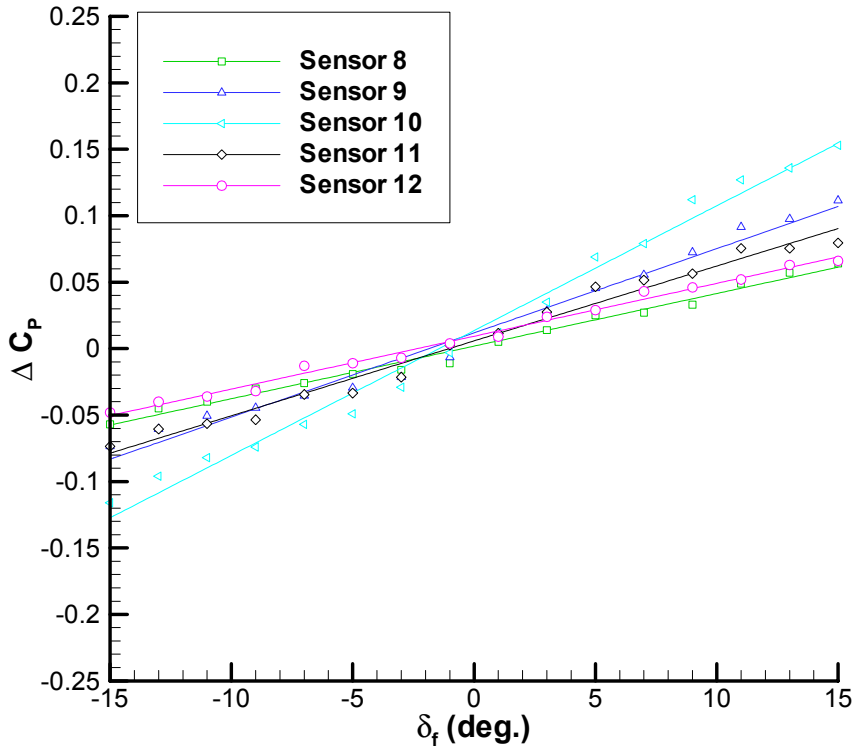

Figure 27: Pressure Response for
Outboard Effector Movement (#10)

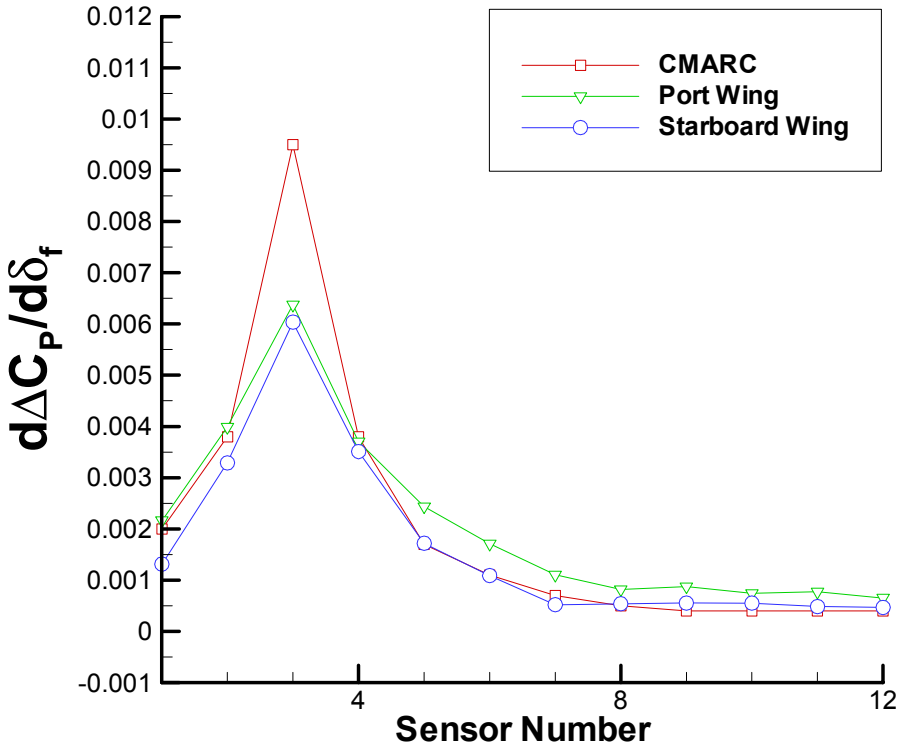

Figure 28: CMARC, Port, and
Starboard Sensitivity Coefficients for
Inboard Effector (#3)

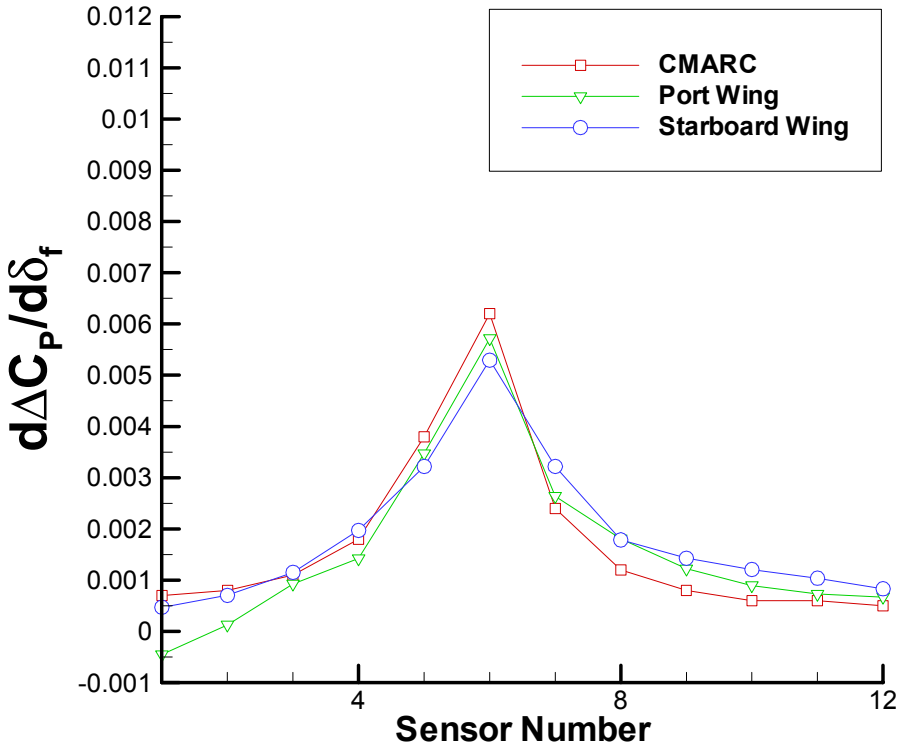

Figure 29: CMARC, Port, and
Starboard Sensitivity Coefficients for
Mid-Span Effector (#6)

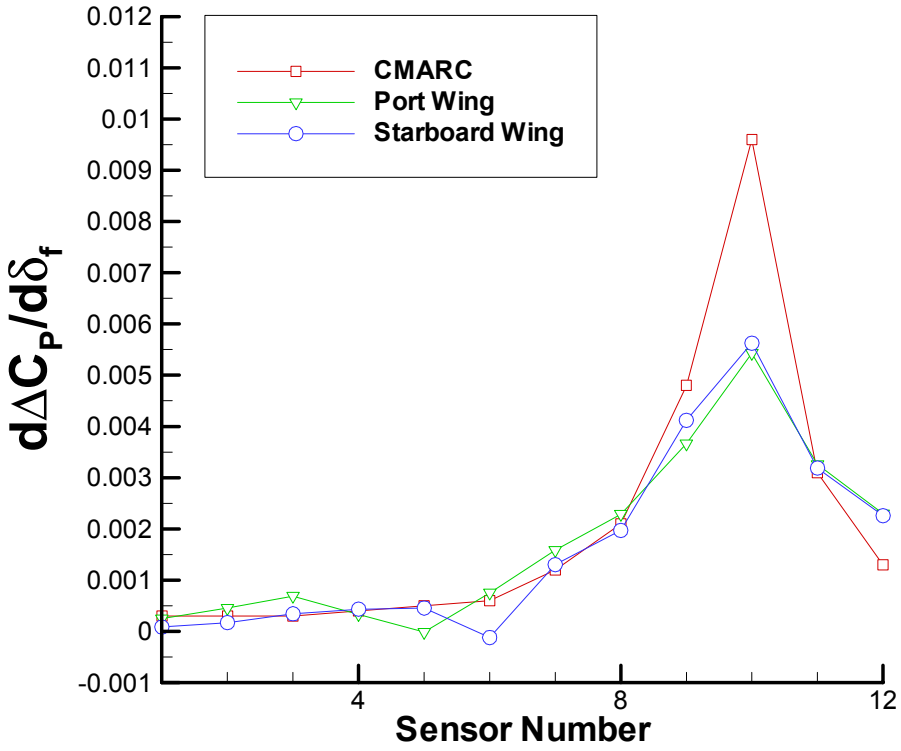

Figure 30: CMARC, Port, and Starboard Sensitivity Coefficients for Outboard Effector (#10)

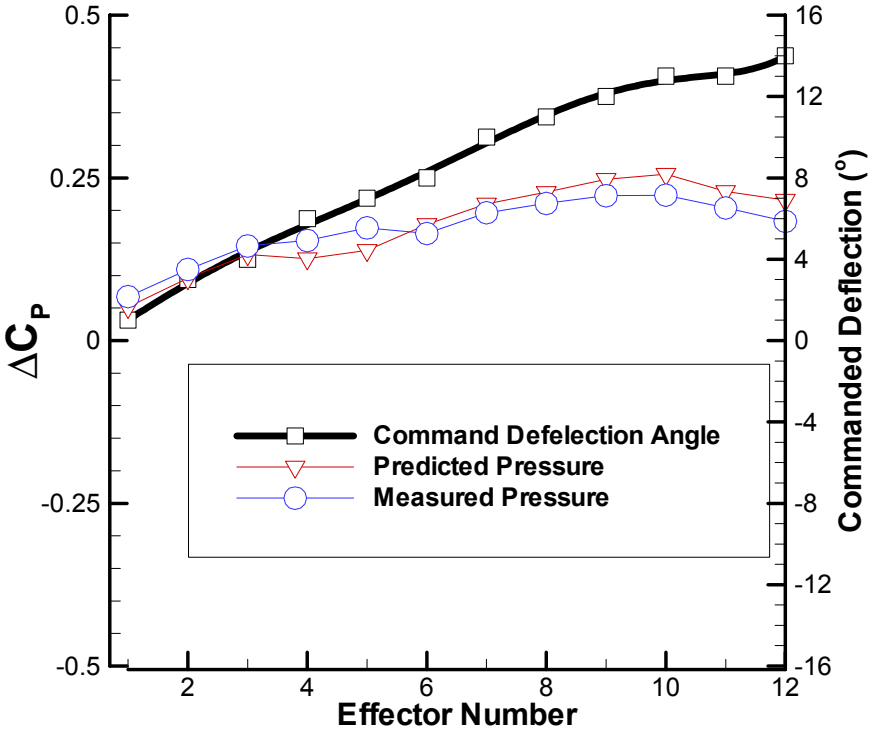

Figure 31: Measured and Predicted Pressure Response for Sine Wave (A = 15°, ω = 0.1)

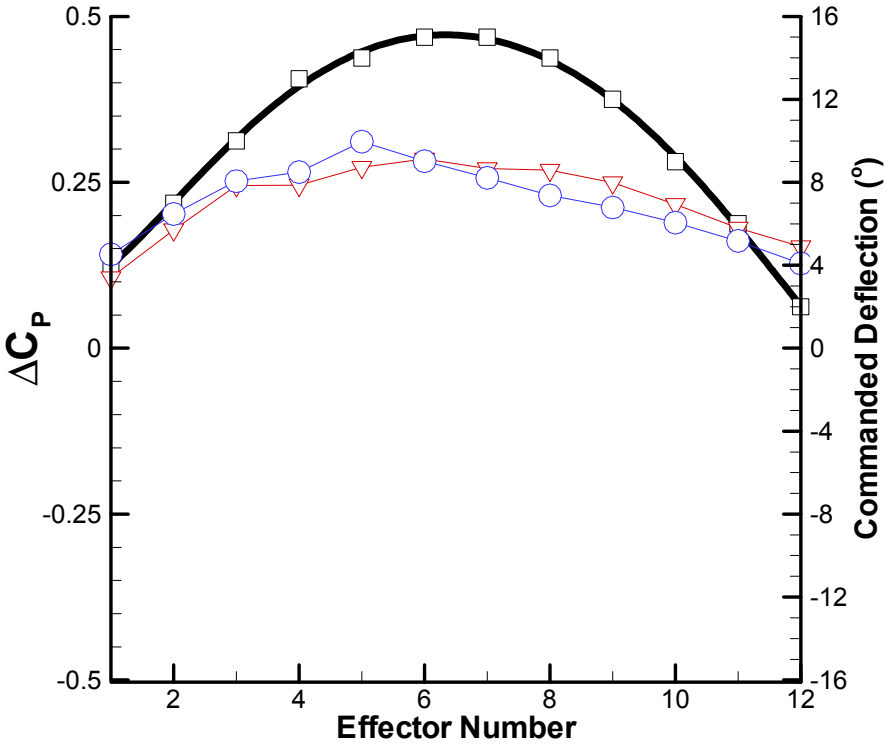

Figure 32: Measured and Predicted Pressure Response for Sine Wave (A = 15°, ω = 0.25)

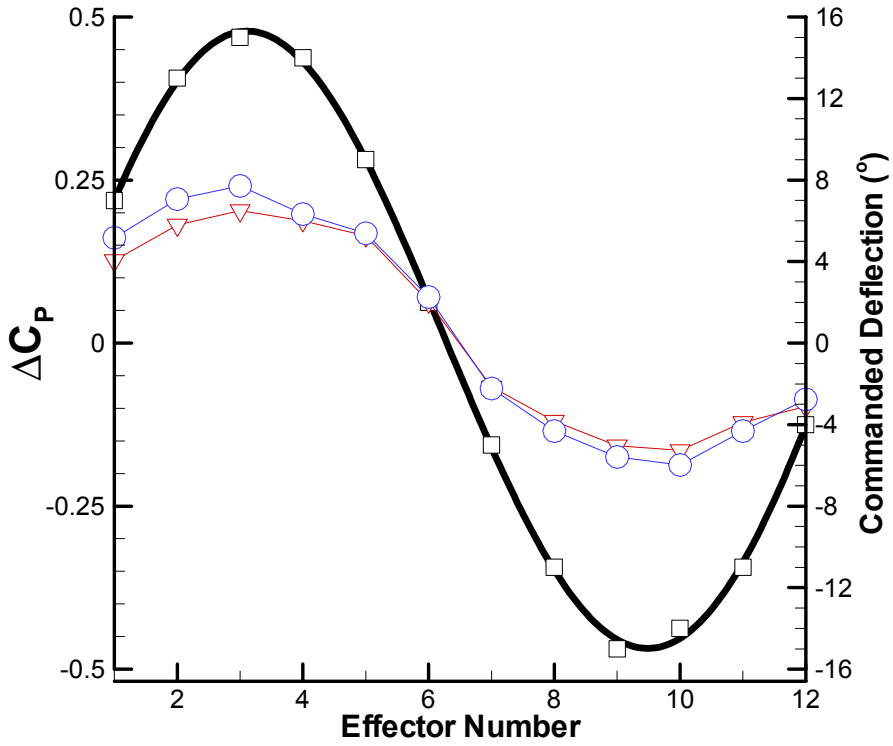

Figure 33: Measured and Predicted Pressure Response for Sine Wave (A = 15°, ω = 0.5)

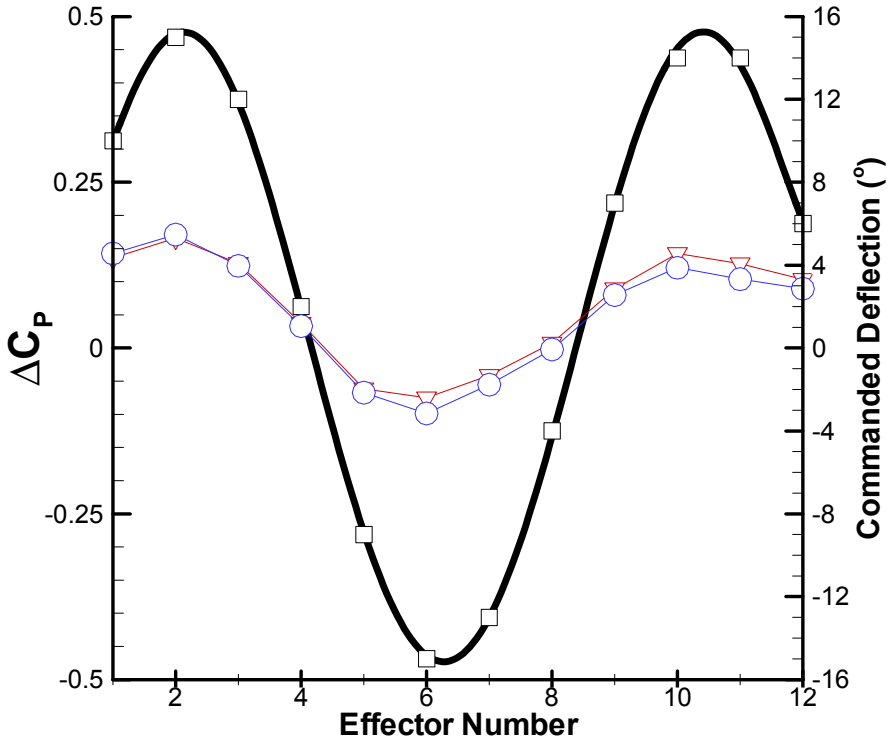

Figure 34: Measured and Predicted Pressure Response for Sine Wave (A = 15°, ω = 0.75)

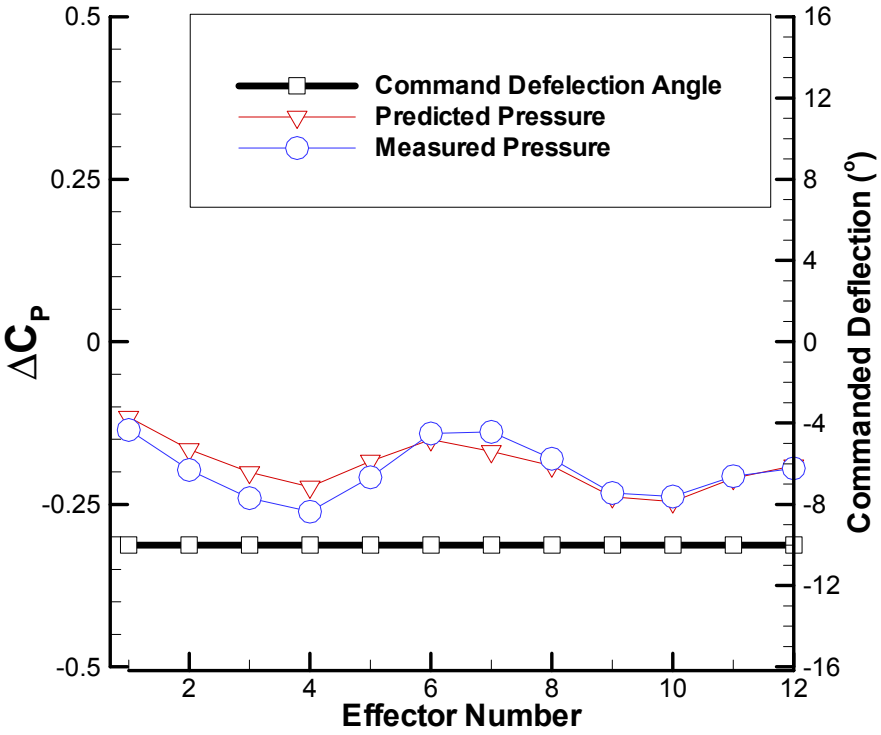

Figure 35: Measured and Predicted Pressure Response for Constant Deflection (A = -10°)

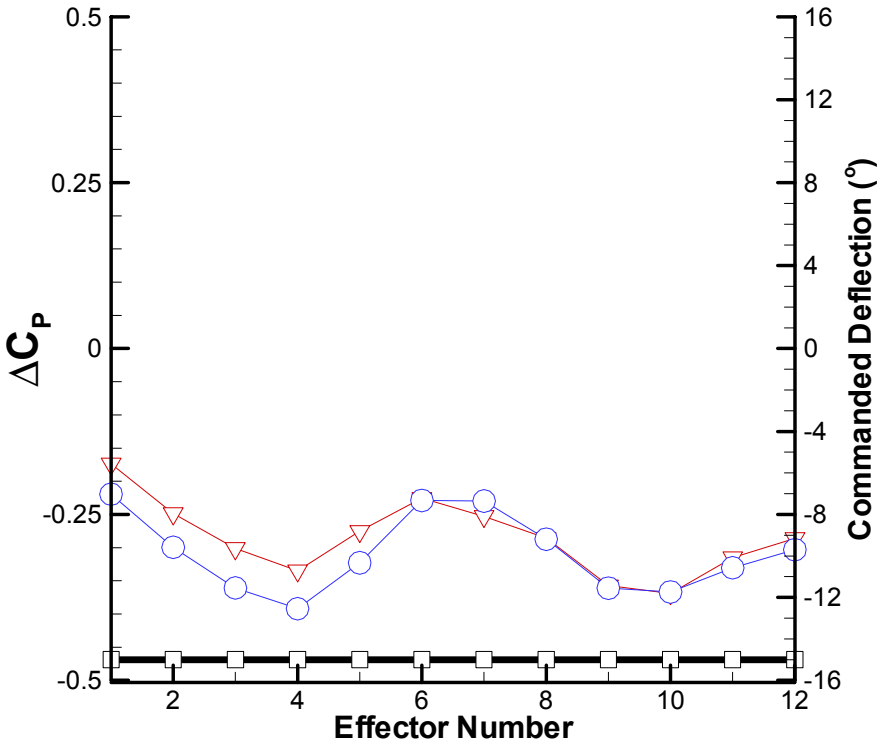

Figure 36: Measured and Predicted Pressure Response for Constant Deflection (A = -15°)

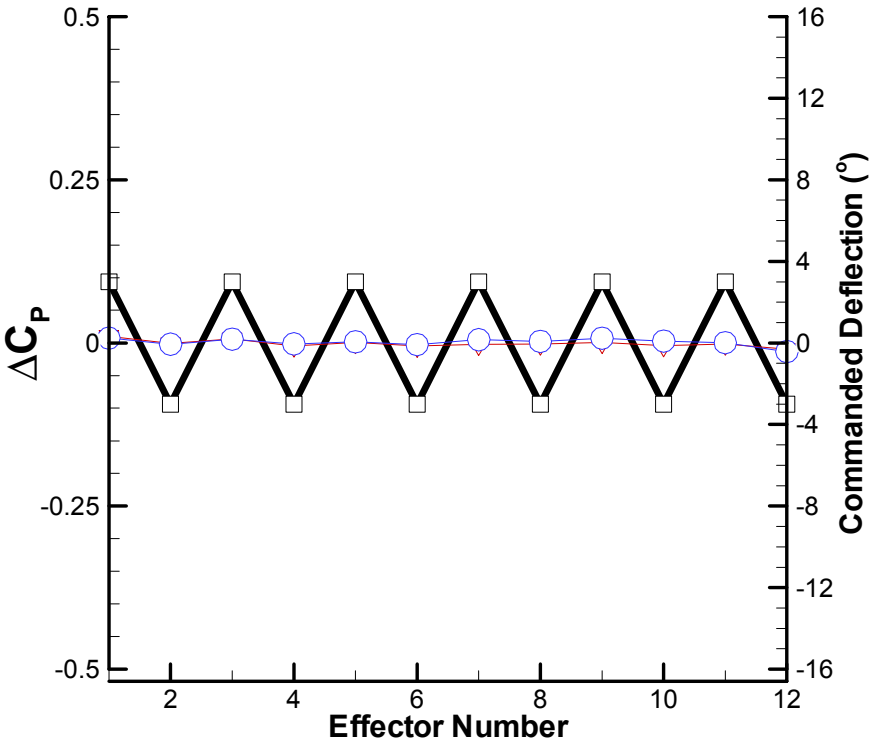

Figure 37: Measured and Predicted Pressure Response for One-Up-One-Down Deflection (A = 4°)

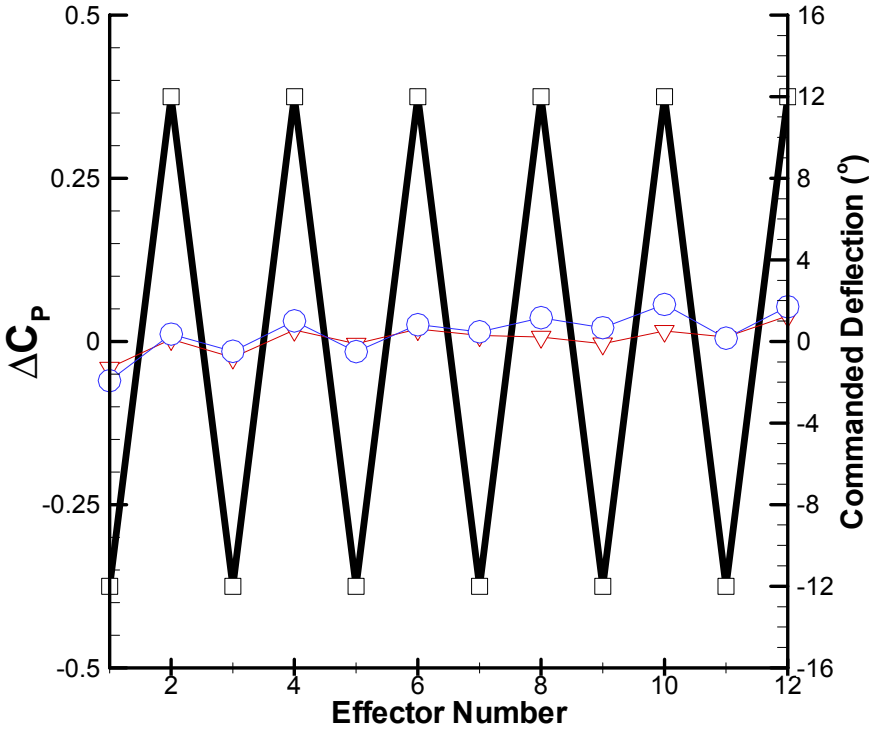

Figure 38: Measured and Predicted Pressure Response for One-Up-One-Down Deflection (A = 12°)

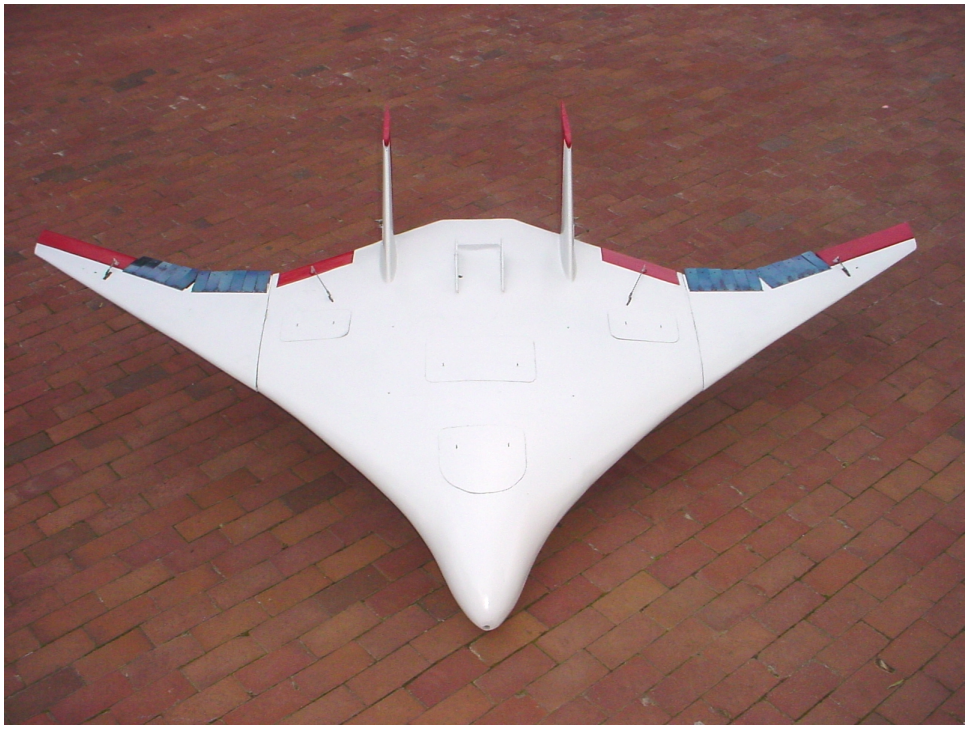

Figure 39: BWB DELTA with
Distributed Effector Wings

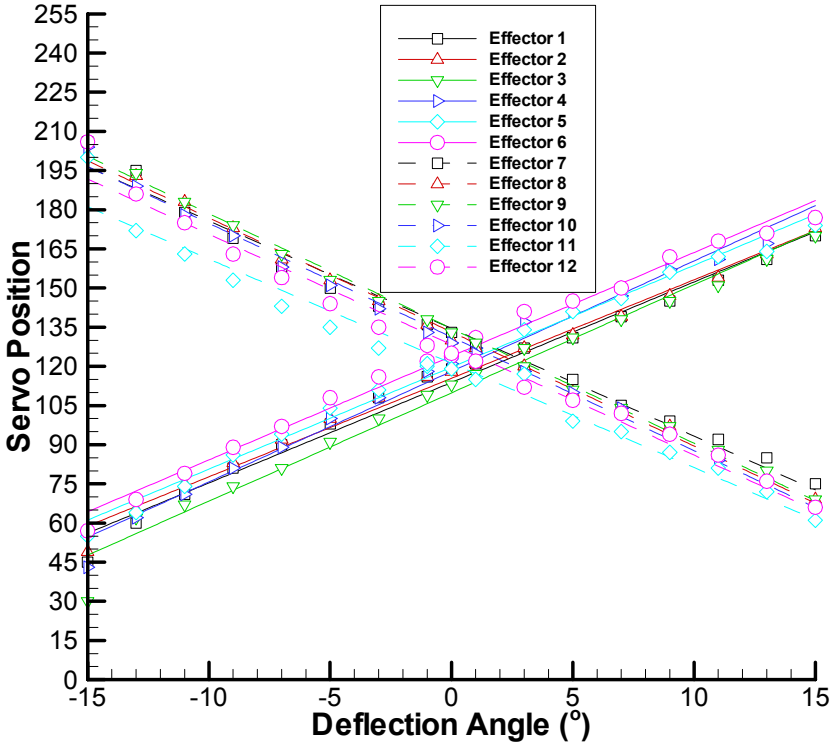

Figure 40: Calibrations for Port Wing

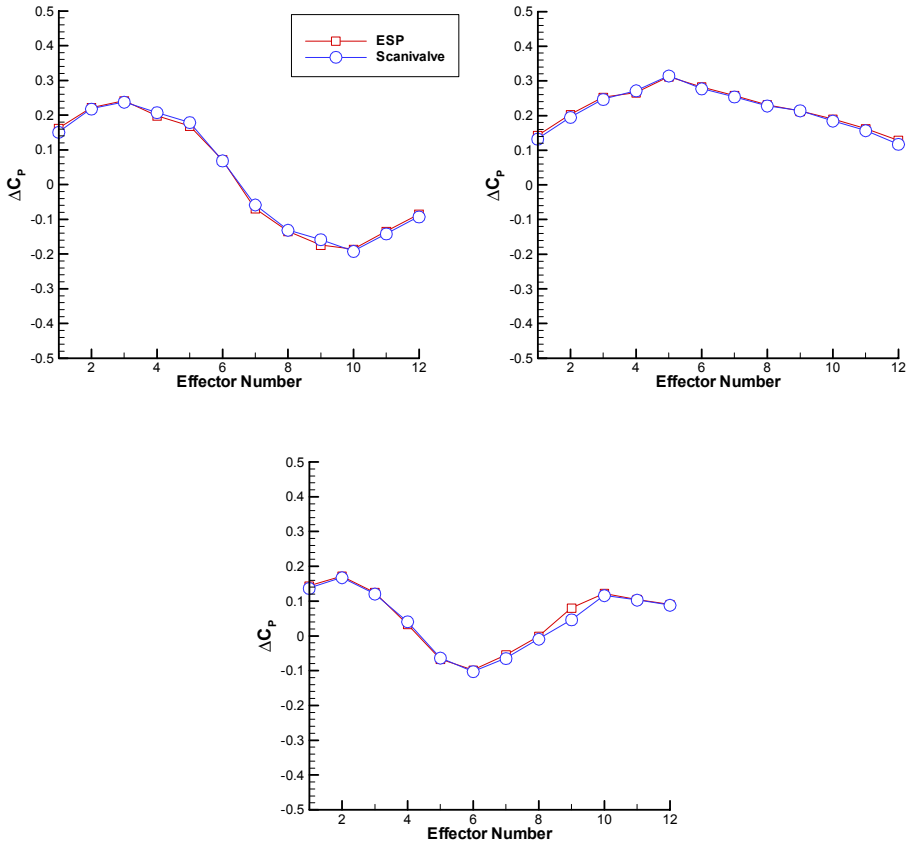

Figure 41: Comparison of ESP vs. Scanivalve

7. BIBLIOGRAPHY

[1] Wlezien, R. W., Horner, G. C., McGowan, A. R., Padula, S. L., Scott, M. A., Silcox, R. J., Simpson, J. O., "The Aircraft Morphing Program," AIAA Paper 98-1927, April 1998.

[2] McGowan, A. R., Horta, L. G., Harrison, J. S., Raney, D. L., "Research Activities within NASA's Morphing Program," NATO RTO Meeting - Applied Vehicle Technology Panel, Ottawa, October 1999.

[3] Ed. Weatherington, D., "Unmanned Aerial Vehicles Roadmap," Office of the Secretary of Defense, December 2002.

[4] Bone, E., Bolkcom, C., "Unmanned Aerial Vehicles: Background and Issues for Congress," *Congressional Research Service Report*, Library of Congress, April 2003.

[5] Sullivan, M., Clark, J., Lea, M., Keener, K., Masters, T., Chaplain, C., Chin, L., Swierczek, B., Rambus, M., "Matching Resources with Requirements is the Key to Unmanned Combat Air Vehicle Program's Success," U.S. General Accounting Office, June 2003.

[6] Blakeslee, R. J., Mach, D. M., Desch, M. D., Goldberg, R. A., Farrell, W. M., Houser, J. G., "The ALTUS Cumulus Electrification Study (ACES): A UAV-Based Science Demonstration," 1st Technical Conference and Workshop on Unmanned Aerospace Vehicles, Systems, Technologies, and Operations, AIAA-2002-3405, May 2002.

[7] Leung, J. G., Higgins, R. G., Dunagan, S. E., Arevesen, J. C., "Remote Command-and-Control of Imaging Payloads Using Commercial Off-the-Shelf Technology," 1st International Geoscience and Remote Sensing Symposium, June 2002.

[8] Herwitz, S. R., Johnson, L. F., Arvesen, J. C., Leung, J. G., Higgins, R. G., Dunagan, S. E., "Precision Agriculture as a Commercial Application for Solar-Powered Unmanned Aerial Vehicles," 1st AIAA UAV Conference, AIAA Paper No. 2002-3404, May 2002.

[9] Youngblood, J. W., Talay, T. A., Pegg, R. J., "Design of Long-Endurance Unmanned Airplanes Incorporating Solar and Fuel Cell Propulsion." AIAA/SAE/ASME 20th Joint Propulsion Conference, Paper No. 84-1430, June 1984.

[10] Teets, E. H., Jr., Donohue, C. J., Underwood, K., Bauer, J. E., "Atmospheric Considerations for Uninhabited Aerial Vehicle (UAV) Flight Test Planning, NASA TM-1998-206541.

[11] Calise, A. J., Johnson, E. N., Johnson, M. D., Corban, J. E., "Applications of Adaptive Neural-Network Control to Unmanned Aerial Vehicles," AIAA/ICAS International Air and Space Symposium and Exposition: The Next 100 Years, Dayton OH, July 2003.

[12] Beard, R. W., McLain, T. W., Goodrich, M., "Coordinated Target Assignment and Intercept for Unmanned Air Vehicles," Proceedings of the 2002 IEEE International Conference on Robotics and Automation, May 2002.

[13] Raney, D. L., Montgomery, R. C., Green, L. L., Park, M. A., "Flight Control Using Distributed Shape-Change Effector Arrays," AIAA Paper 2000-1560, April 2000.

[14] Gad-el-Hak, M., "Flow Control: Passive, Active and Reactive Flow Management," Cambridge University Press, Cambridge United Kingdom, 2000.

[15] Fontenrose, P. L., Hall Jr., C. E., "Development and Flight Testing of Quantitative Feedback Theory Pitch Rate Stability Augmentation System" Journal of Guidance, Control and Dynamics, Vol. 19, September-October 1996, pp. 1109-1115.

[16] Heinzen, S. N., Hall Jr., C. E., Chokani, N., "In-Flight Application of Active Separation Control Using Pulsed Jet Blowing" AIAA Paper 2002-0416, January 2002.

[17] Krozel, J., Peters, M., "Decentralized Control Techniques for Distributed Air/Ground Traffic Separation," NASA TR 99RTO36-03, June 2000.

[18] Stipanovic, D. M., Inalhan, G., Teo, R., Tomlin, C. J., "Decentralized Overlapping Control of a Formation of Unmanned Aerial Vehicles," Proc. Of the 41st IEEE Conference on Decision and Control, December 2002.

[19] Bamieh, B., Paganini, F., Dahleh, M. A., "Distributed Control of Spatially Invariant Systems," IEEE Transactions on Automatic Control, Vol. 47, No.7, July 2002.

[20] Kroo, I., "Aerodynamic Concepts for Future Aircraft," AIAA Paper 99-3524, July 1999.

[21] D'Andrea, R., "A Linear Matrix Inequality Approach to Decentralized Control of Distributed Parameter Systems," Proc. IEEE Conference on Decision and Control, pp. 1056-1071, 1997.

[22] Kudva, J. N., Appa, K., Van Way, C. B., Lockyer, A. J., "Adaptive Smart Wing Design for Military Aircraft" Requirements and Payofffs," Paper No. 2716-10, SPIE North American Conference on "Smart Structures and Materials." San Diego, CA, February, 1996.

[23] Kudva, J. N., Appa, K., Martin, C.A., Jardine, A. P., Carpenter, B. F., "Overview of recent progress on the DARPA/USAF Wright Laboratory "Smart Materials and Structures Smart Wing" program" SPIE Vol. 3044, No. 3044-01, March 1997.

[24] Scherer, L. B., Martin, C. A., Appa, K., Kudva, J. N., "Smart Wing Wind Tunnel Test Results", Paper No. 3044-05, SPIE Symposium on Smart Materials and Structures, March 4 1997.

[25] Hoadley, A., Pederson, E., "Prediction of Airfoil Stall in Icing Conditions Using Wing Surface Pressures," *AIAA Paper 2001-0422*, January 2001.

[26] Liebeck, R. H., Page, M.A. "Evolution of the Revolutionary Blended-Wing-Body", NASA Center for Aerospace Information. 1996

[27] "UAV *Thunderstruck*: Fall Report," NC State University Senior Aircraft Design Class: Fall Report, December 2001.

[28] "UAV *Thunderstruck:* Spring Report" NC State University Senior Aircraft Design Class: Spring Report, May 2002.

[29] Drela, M., "XFOIL: An Analysis and Design System for Low Reynolds Number Airfoils," Conference on Low Reynolds Number Airfoil Aerodynamics, University of Notre Dame, June 1989.

[30] Ashby, D. L., Dudley, M. R., Iguchi, S. K., Browne, L., Katz, J., "Potential Flow Theory and Operation Guide for the Panel Code PMARC," NASA TM-102851, January 1991.

[31] Hall, C.E. Private Communication, September 2000.

[32] Sloan, A. R., Raney, D. L., Private Communication, August 2002.